Effect of Glycosylation on MUC1 Humoral Immune Recognition: NMR Studies of MUC1 Glycopeptide−Antibody Interactions†

Jeffrey S. Grinstead,‡ R. Rao Koganty,§ Mark J. Krantz,§ B. Michael Longenecker,§ and A. Patricia Campbell*,‡

Department of Medicinal Chemistry, School of Pharmacy, University of Washington, Seattle, Washington 98195, and Biomira Inc., 2011-94 Street, Edmonton, Alberta, Canada T6N 1H1

Received December 19, 2001

ABSTRACT: MUC1 mucin is a large transmembrane glycoprotein, of which the extracellular domain is formed by a repeating 20 amino acid sequence, GVTSA**PDTRP**APGSTAPPAH. In normal breast epithelial cells, the extracellular domain is densely covered with highly branched complex carbohydrate structures. However, in neoplastic breast tissue, the extracellular domain is underglycosylated, resulting in the exposure of a highly immunogenic core peptide epitope (PDTRP in bold above) as well as the normally cryptic core Tn (GalNAc), STn (sialyl α2−6 GalNAc), and TF (Gal β1−3 GalNAc) carbohydrates. In the present study, NMR methods were used to correlate the effects of cryptic glycosylation outside of the PDTRP core epitope region to the recognition and binding of a monoclonal antibody, Mab B27.29, raised against the intact tumor-associated MUC1 mucin. Four peptides were studied: a MUC1 16mer peptide of the sequence Gly1-Val2-Thr3-Ser4-Ala5-Pro6-Asp7-Thr8-Arg9-Pro10-Ala11-Pro12-Gly13-Ser14-Thr15-Ala16, two singly Tn-glycosylated versions of this peptide at either Thr3 or Ser4, and a doubly Tn-glycosylated version at both Thr3 and Ser4. The results of these studies showed that the B27.29 MUC1 B-cell epitope maps to two separate parts of the glycopeptide, the core peptide epitope spanning the PDTRP sequence and a second (carbohydrate) epitope comprised of the Tn moieties attached at Thr3 and Ser4. The implications of these results are discussed within the framework of developing a glycosylated second-generation MUC1 glycopeptide vaccine.

Mucins are attracting real interest as potential targets in the development of vaccines for adenocarcinomas expressing mucin 1 (MUC1),[1] particularly for breast cancer but also for pancreatic, lung, colorectal, and ovarian cancers (*1*−*4*). MUC1 mucin is a large transmembrane glycoprotein, of which the extracellular domain is formed by a repeating 20 amino acid sequence (GVTSA**PDTRP**APGSTAPPAH)$_n$. In normal breast epithelial cells, the extracellular domain is densely covered with highly branched complex carbohydrate structures, attached to the proximal serine and threonine residues within the peptide sequence (*5*−*8*). However, in the tumor-associated state, MUC1 becomes an autoantigen as a result of incomplete glycosylation and sparse distribution of these carbohydrate structures (*9*). This is believed to result in the exposure of a highly immunogenic core peptide sequence (PDTRP in bold above) (*10*) identified as the immunodominant B-cell epitope from monoclonal antibody studies in mice (*11*−*16*). Abnormal glycosylation is also believed to result in the exposure of the normally cryptic core Tn (GalNAc), STn (sialyl α2−6 GalNAc), and TF (Gal β1−3 GalNAc) carbohydrates (*17, 18*). All three carbohydrate epitopes are strongly expressed on human carcinoma cells (*17, 19*−*22*) and may be associated with cancer progression and metastasis (*23*−*25*).

There are five potential O-glycosylation sites in each tandem repeat of the MUC1 sequence (GVTSAPDTRPAPGSTAPPAH). Identifying which of these sites remains glycosylated in the tumor-associated state is important for MUC1 vaccine design, as the vaccine should approximate as closely as possible the glycosylation state and peptide backbone exposure of the intact tumor. In vitro glycosylation studies using human tumor cell extracts (*26*, *27*) and three different recombinant GalNAc transferases identified from human tumor cell lines (*28*) have demonstrated glycosylation at three separarate sites (GVTSA and GSTAP) but not at the threonine within the PDTRP core peptide epitope region. These findings are significant insofar as reduced glycosylation of MUC1 is assumed to permit the immune system access to this region of the peptide sequence. However, recent in vivo studies have demonstrated that all five sites on the MUC1 tandem repeat are glycosylation targets (*29*, *30*), although there is no evidence to suggest that all sites are actually glycosylated.

† This work was funded by a U.S. Army Breast Cancer Grant (DAMD17-99-1-9437) and by the American Association of Colleges of Pharmacy.

* To whom correspondence should be addressed. Tel: (206) 685-2468. Fax: (206) 685-3252. E-mail: apc@u.washington.edu.

‡ University of Washington.

§ Biomira Inc.

[1] Abbreviations: CD, circular dichroism; DQFCOSY, double-quantum filtered coherence spectroscopy; DSS, 2,2-dimethyl-2-sila-5-pentanesulfonate; ELISA, enzyme-linked immunosorbent assay; Fab, antigen-binding fragment of monoclonal antibody; GalNAc, α-*N*-acetylgalactosamine; HSQC, heteronuclear single-quantum coherence spectrum; Mab, monoclonal antibody; MUC1, mucin 1; NMR, nuclear magnetic resonance; NOE, nuclear Overhauser effect; NOESY, 2D nuclear Overhauser effect spectroscopy; STn, sialyl-Tn; TF, Thomsen−Friedenriech; TOCSY, total correlation spectroscopy.

10.1021/bi012176z CCC: $22.00
Published on Web 07/13/2002

In a recent study by this group, NMR methods were used to probe the structural and dynamical consequences of glycosylation at the central threonine within the PDTRP core epitope region of MUC1 synthetic peptides (*31*). This study showed that a well-populated type I β-turn was adopted by residues PDTR in the unglycosylated MUC1 sequence and that attachment of a Tn carbohydrate to the central threonine within this sequence resulted in a destabilization of the β-turn and a shift in the conformational equilibrium of the underlying peptide backbone toward a more rigid and extended state. The existence of a similar β-turn within the PDTRP core peptide epitope of the underglycosylated tumor-associated MUC1 mucin protein might explain the immunodominance of this region in vivo, as the presence of β-turn structure has been correlated with increased immunogenicity in other systems.

In the present study, we use NMR methods to probe the structural and dynamical consequences of glycosylation at serine and threonine residues upstream of the PDTRP core epitope region of MUC1 synthetic peptides and correlate these effects to the recognition and binding of a monoclonal antibody, Mab B27.29,[2] raised against the intact tumor-associated MUC1 mucin. Four peptides were studied: a MUC1 16mer peptide of the sequence Gly1-Val2-Thr3-Ser4-Ala5-Pro6-Asp7-Thr8-Arg9-Pro10-Ala11-Pro12-Gly13-Ser14-Thr15-Ala16, two singly Tn-glycosylated versions of this peptide at either Thr3 or Ser4, and a doubly Tn-glycosylated version at both Thr3 and Ser4. Included in the study are two-dimensional ^{1}H NMR TRNOESY studies of the binding of the doubly glycosylated MUC1 16mer to the Fab fragment of B27.29, so as to allow a mapping of the MUC1 B-cell epitope, and an assessment of the contribution of the PDTRP core peptide epitope versus the Tn core carbohydrate epitope to Mab B27.29 recognition and binding. The results of these studies are discussed within the framework of developing a glycosylated second-generation MUC1 glycopeptide vaccine.

EXPERIMENTAL PROCEDURES

MUC1 Peptides and Fab B27.29. MUC1 peptides and glycopeptides were provided by Biomira Inc., Edmonton, Alberta, Canada. These included an unglycosylated 16mer (Gly1-Val2-Thr3-Ser4-Ala5-Pro6-Asp7-Thr8-Arg9-Pro10-Ala11-Pro12-Gly13-Ser14-Thr15-Ala16), two singly glycosylated versions of this 16mer, one with a Tn carbohydrate α-linked to the β-hydroxyl of Thr3 (Tn3-glycosylated 16mer) and the other with the Tn carbohydrate α-linked to the β-hydroxyl of Ser4 (Tn4-glycosylated 16mer), and a doubly glycosylated version of the 16mer, with Tn carbohydrates α-linked to the β-hydroxyls of both Thr3 and Ser4 (Tn3,Tn4-glycosylated 16mer). The Fab fragment of anti-MUC1 monoclonal antibody B27.29 was prepared by papain digestion of the purified intact IgG and was also provided in lyophilized form by Biomira Inc.

2D ^{1}H NMR Spectroscopy of MUC1 Peptides Free in Solution. Peptide NMR samples of the unglycosylated 16mer, Tn3-glycosylated 16mer, Tn4-glycosylated 16mer, and Tn3,Tn4-glycosylated 16mer were prepared by dissolving the lyophilized peptides in 450 μL of 90% H_2O/10% D_2O PBS buffer to a concentration of 1 mM by mass. DSS was then added as an internal chemical shift reference, and the final pH was adjusted to 7.0. ^{1}H NMR experiments were acquired at 500 MHz on a Varian Inova 500 spectrometer equipped with an actively shielded *z*-axis gradient and a triple resonance probe. The hypercomplex method (*35*) was used for acquisition of all 2D data sets. DQFCOSY (*36*, *37*) and TOCSY (*38*) data sets typically included 6000 Hz spectral widths, 64 transients, 300 increments, and 4096 points along F_2, whereas NOESY (*39*, *40*) data sets typically included 6000 Hz spectral widths, 256 transients, 256 increments, and 2048 points along F_2. TOCSY experiments utilized a spin lock field of 7.12 kHz. NOESY experiments were acquired with a mixing time of 300 ms. All 2D data sets were collected in duplicate at two separate temperatures: 5 °C to retard rapid backbone amide proton exchange and 25 °C to temperature shift the water peak and allow observation of carbohydrate resonances between 4.7 and 5.0 ppm. Water suppression was achieved using a gradient-tailored echo pulse sequence incorporating two selective pulses around the 180° pulse of the echo that prevent the water signal from refocusing. In addition, a water selective 90° pulse followed by a gradient was used to diffuse water. 2D data sets were processed on a SGI Octane workstation using NMRPipe/NMRDraw software (*41*). Typical processing utilized 90°-shifted sine-bell squared window functions and zero filling to 4K × 4K prior to Fourier transformation.

Temperature coefficients ($-\Delta\delta/\Delta T$, ppb) for all backbone amide (NH) protons of the unglycosylated and Tn-glycosylated MUC1 16mers were calculated from linear plots of NH chemical shift versus temperature. The NH chemical shifts were measured from DQFCOSY spectra acquired at 5 and 25 °C and from one-dimensional spectra acquired at 5, 10, 15, 20, and 25 °C. $^3J_{N\alpha}$ coupling constants were obtained from the backbone NH proton region of the one-dimensional spectra acquired at 5 °C, where the individual resonances were curve-fitted using a program written by R. Boyko (University of Alberta; xcrvfit program available at www.pence.ualberta.ca.ftp) which utilizes an iterative fitting procedure. Where overlap of the NH resonances in the one-dimensional spectrum precluded analysis, $^3J_{N\alpha}$ coupling constants were obtained from the αCH−NH fingerprint region of the 4K × 4K ($F_2 \times F_1$) DQFCOSY spectrum acquired at 5 °C. The DQFCOSY spectrum was zero filled to 16K in the F_2 dimension and processed using 90°-shifted sine-bell weighting in the F_1 dimension and no weighting in the F_2 dimension. Traces were taken in ω_2 and then curve-fitted as described above.

Natural Abundance $^{13}C\alpha$ Relaxation Measurements of MUC1 Peptides Free in Solution. 500 MHz $^{13}C\alpha$ T_1 and $^{13}C\alpha$ $T_{1\rho}$ relaxation times and steady-state $\{^1H\alpha\}-^{13}C\alpha$ heteronuclear NOE values were measured for the unglycosylated and Tn3,Tn4-glycosylated 16mers to determine the effect of glycosylation on local backbone motion. NMR samples were prepared by dissolving the peptides in 500 μL of 99.9% D_2O PBS buffer, pH 7.0, to a concentration of 10 mM. The pulse sequences of Yamakazi and co-workers (*42*) were used for these measurements, modified to remove ^{15}N and $^{13}C'$ decoupling. ^{13}C broad-band decoupling during acquisition

[2] Monoclonal antibody B27.29 was raised against ovarian tumor cell derived mucin and displays specificity for MUC1 expressing tumors of the ovaries and breast (*32*). Epitope fingerprinting studies identify the B27.29 epitope as PDTRPAP (GVTSA**PDTRPAP**GSTAPPAH) within the immunodominant PDTRP epitope region (*33*). B27.29 is used as a diagnostic antibody for cancer expressing the MUC1 mucin (*34*).

was achieved using GARP, with a field strength of 8.2 kHz. Relaxation delays of 5, 50, 100, 150, 200, 300, 400, 500, and 600 ms were used for the T_1 experiments, and delays of 4.0, 8.0, 12.1, 16.1, 24.1, 40.2, 56.3, and 80.0 ms were used for the $T_{1\rho}$ experiments. Both the T_1 and $T_{1\rho}$ experiments used a recycling delay of 1.2 s between transients. The $\{^1H\alpha\}-^{13}C\alpha$ NOE was obtained by recording spectra with and without 3 s of ^1H saturation. In the case of spectra acquired without NOE, a net recycling delay of 5 s was employed, whereas a recycling delay of 2 s prior to 3 s of ^1H saturation was employed for spectra with NOE. All T_1, $T_{1\rho}$, and NOE spectra were recorded at 5 °C using spectral widths of 6000 and 2500 Hz for ^1H and ^{13}C, respectively, 105 increments in the ^{13}C dimension, and 1024 complex points per FID.

$^{13}C\alpha$ T_1, $T_{1\rho}$, and NOE data sets were processed on a SGI Octane workstation using NMRPipe/NMRDraw software (*41*). The FID's in the ^{13}C dimension were doubled using forward linear prediction. Typically, spectra were processed in the acquisition and indirect dimensions with 90°-shifted sine-bell squared window functions. For the ^{13}C T_1 and $T_{1\rho}$ data sets, a Lorentz-to-Gauss transformation was performed. NMRPipe/NMRDraw software was used to pick peaks and fit the measured peak heights to a two-parameter exponential decay function of the form

$$I(t) = I_0 \exp(-t/T_{1,1\rho}) \quad (1)$$

where $I(t)$ is the intensity after a delay of time t and I_0 is the intensity at time $t = 0$. The uncertainties in the T_1 and $T_{1\rho}$ values from nonlinear least-squares fit were calculated using the assumption that the RMS noise in each spectrum gives a good estimation of the error in the measured intensities of the peaks. This assumption was validated by comparison of two experiments with identical relaxation times, where the standard deviation of the peak heights was shown to approximate $\sqrt{2} \times$ RMS noise in each of the spectra.

The steady-state $\{^1H\}-^{13}C$ NOE values were determined from the ratios of the average intensities of the peaks with and without ^1H saturation. The standard deviation of the NOE value, σ_{NOE}, was determined on the basis of measured background noise levels using the relationship

$$\sigma_{NOE}/NOE = [(\sigma_{I_{sat}}/I_{sat})^2 + (\sigma_{I_{unsat}}/I_{unsat})^2]^{1/2} \quad (2)$$

where I_{sat} and I_{unsat} represent the measured intensities of a resonance in the presence and absence of proton saturation, respectively. The standard deviations of these values, estimated from the root-mean-square noise of background regions, are represented by $\sigma_{I_{sat}}$ and $\sigma_{I_{unsat}}$.

Fluorescence Measurements of MUC1 Peptides Binding to Fab B27.29. Fluorescence measurements were used to determine the equilibrium dissociation constants (K_D) and off-rates (k_{off}) for the binding of the unglycosylated 16mer, Tn3-glycosylated 16mer, Tn4-glycosylated 16mer, and Tn3,Tn4-glycosylated 16mer peptides to Fab B27.29. Fab B27.29 (0.86 μM stock solution) was titrated with small aliquots of peptide and glycopeptide to a final concentration greater than 200-fold in excess of Fab concentration. The change in Fab fluorescence intensity was monitored, and the concentration of bound ligand was calculated (percent of maximum fluorescence change). The natural log of the free ligand concentration was plotted against the concentration of the bound ligand, and the curve was fit to the equation

$$[\text{bound}] = (\text{capacity}[\text{free ligand}])/(K_D + [\text{free ligand}]) \quad (3)$$

according to Michaelis−Menten kinetics, where the capacity is the concentration of the Fab and the K_D is the equilibrium dissociation constant.

^1H NMR-Monitored Titrations of MUC1 Peptides with Fab B27.29. ^1H NMR-monitored titrations of the unglycosylated 16mer and the Tn3,Tn4-glycosylated 16mer with Fab B27.29 were next undertaken. These included forward titrations (peptide NMR sample titrated with Fab) and reverse titrations (Fab NMR sample titrated with peptide), so as to correct for any nonspecific line broadening of peptide resonances caused by Fab-induced increases in sample viscosity. The forward titrations used the 1 mM peptide NMR samples prepared above in 90% H_2O/10% D_2O PBS buffer. Lyophilized Fab was added to these peptide NMR samples in small aliquots of a few milligrams at a time to a final concentration of 400 μM (0.4 molar equiv of Fab/peptide). In the reverse titration, lyophilized Fab was dissolved in 450 μL 90% H_2O/10% D_2O PBS buffer, pH 7.0, to a concentration of 200 μM by mass. Peptide was then added in aliquots of 10−20 μL from an 8 mM stock solution to a final concentration of 1.4 mM (0.14 molar equiv of Fab/peptide). All NMR samples contained DSS as an internal chemical shift reference, and the pH was adjusted to within 7.0 ± 0.05 after each aliquot of peptide or Fab was added.

One-dimensional ^1H NMR data sets were collected at four points in each of the forward and reverse titrations. In the forward titration, these points represented 0 μM Fab (1 mM free peptide), 100 μM Fab (0.1 molar equiv of Fab/peptide), 200 μM Fab (0.2 molar equiv of Fab/peptide), and 400 μM Fab (0.4 molar equiv of Fab/peptide). In the reverse titration, these points represented 0 μM peptide (200 μM free Fab), 400 μM peptide (0.5 molar equiv of Fab/peptide), 800 μM peptide (0.25 molar equiv of Fab/peptide), and 1.4 mM peptide (0.14 molar equiv of Fab/peptide). NOESY and TRNOESY data sets were acquired at 5 and 25 °C for the beginning and end point of the forward titration and for all four points in the reverse titration. DQFCOSY data sets were acquired at 5, 10, 15, 20, and 25 °C for the beginning and end points of the forward titration. Data acquisition and processing details for these NMR experiments have been described earlier in Experimental Procedures, as have the methodologies for calculation of temperature coefficients and $^3J_{N\alpha}$ coupling constants from the DQFCOSY data sets.

Determination of Exchange Time Scales for the Binding of the MUC1 Peptides to Fab B27.29. Interpreting ^1H NMR results for systems undergoing chemical exchange (for example, the MUC1 peptides binding to Fab B27.29) requires a determination of exchange time scales with respect to both chemical shift and T_1 relaxation. BIAcore analysis of the binding of a one-repeat unglycosylated MUC1 peptide to Mab B27.29 has measured a $K_D = 63$ nM (*43*). Since most Fab fragments have K_D's 10−20-fold higher than their parent IgG's (reflecting differences in avidity due to monovalent binding; *44*), the K_D for the binding of the same one-repeat peptide to Fab B27.29 is expected to be in the range of $0.1 \leq K_D \leq 1$ μM. Our own fluorescence measurements of the

MUC1 16mer peptides and glycopeptides binding to Fab B27.29 have produced K_D's in the range of 10 ± 10 μM, in rough agreement with these calculations. Assuming a $K_D \approx 1$ μM and a diffusion-controlled on-rate ($k_{on} = 10^8$ M^{-1} s^{-1}), k_{off} is then calculated to be $\sim$100 s^{-1}, or 100 Hz. Typical differences between free and bound chemical shifts are 100−1000 Hz (45), so a $k_{off} = 100$ Hz places the MUC1 system into intermediate exchange on the chemical shift time scale. In this regime, resonances do not shift with varying concentration of ligand but instead experience a loss in signal intensity due to line broadening (*45*). This is the behavior exhibited in our NMR titrations of MUC1 peptides and glycopeptides binding to Fab B27.29 (see Results).

It is appropriate to note here that the line broadening observed in the MUC1 peptide−Fab titrations is only partly caused by intermediate exchange chemical shift behavior. Changes in the relaxation properties of MUC1 peptide backbone and side chain resonances as these regions are bound and partially immobilized within the antibody combining site also contribute to line broadening effects. Indeed, NMR relaxation measurements of MUC1 peptides in the presence of Fab have demonstrated a strong correlation between Fab-induced line broadening and Fab-induced decreases in T_1 (manuscript in preparation), indicating decreased mobilities for broadened resonances and, more importantly, fast exchange on the relaxation time scale. The existence of these two exchange regimes for the MUC1 system, intermediate on the chemical shift time scale but fast on the relaxation time scale, allows implementation of TRNOESY experiments (see below) which rely on changes in T_1 to relay information of the bound state.

TRNOESY Studies of the Binding of MUC1 Peptides to Fab B27.29. The transferred nuclear Overhauser effect (TRNOE) is an extension of the nuclear Overhauser effect (NOE) to exchanging systems such as peptide−protein complexes (*46*). In the presence of chemical exchange, NOEs conveying conformational information of the bound peptide are "transferred" to the free peptide resonances. Equation 4 diagrammatically represents a system undergoing chemical exchange, in this case a MUC1 16mer peptide binding to Fab 27.29. Here, P_F and P_B are the free and bound peptide, k_1[Fab] and k_{-1} are the exchange rates, τ_F and τ_B are the correlation times which modulate the interaction between protons in the free and bound peptide, and W_F and W_B are the dipolar cross-relaxation rates between protons in the free and bound peptide (proportional to the measured NOE intensities, NOE_F and NOE_B, at short mixing times):

$$\begin{array}{ccc} \text{Fab} + P_F & \underset{k_{-1}}{\overset{k_1[\text{Fab}]}{\rightleftharpoons}} & \text{Fab}\cdot P_B \\ \tau_F \approx 10^{-9}\,\text{s} & & \tau_B > 10^{-9}\,\text{s} \\ W_F \propto \text{NOE}_F & & W_B \propto \text{NOE}_B \end{array} \quad (4)$$

The only necessary condition for the transfer of magnetization is that the exchange rate be faster than the T_1 longitudinal relaxation rate of the bound peptide ($k_{-1} > 1/T_{1B}$), i.e., fast exchange with respect to relaxation. This condition is met in the MUC1 system studied. Under these conditions, the TRNOE is dominated by the bound peptide conformation (even for $P_F > P_B$), since the cross-relaxation rates for the bound peptide are so much faster than they are for the free ($W_B \gg W_F$). However, since the MUC1 system is also in intermediate exchange with respect to chemical shift, the measured TRNOE cannot be simply deconvoluted into a populated weighted average of free and bound NOEs (*46*). Thus, a qualitative as opposed to a quantitative approach must be adopted in analyzing the TRNOE results obtained for the MUC1 system.

Modeling of a Proposed Antibody Binding Interface on the MUC1 Glycopeptide. Peptide−Fab and sugar−Fab NOEs observed in the TRNOESY studies of the Tn3,Tn4-glycosylated 16mer binding to Fab B27.29 were used to model a proposed antibody binding interface on the MUC1 glycopeptide. Modeling was performed on a SGI Octane using the BIOPOLYMER and DISCOVER modules within the Insight II program (Molecular Simulations Inc., San Diego, CA). The protocol involved the following three steps:

(1) Select residues in the Tn3,Tn4-glycosylated 16mer were set to defined ϕ and ψ values, which remained fixed throughout subsequent steps. Asp7 and Thr8 were set to a type I β-turn conformation ($\phi_2 = -60°$, $\psi_2 = -30°$, $\phi_3 = -90°$, $\psi_3 = 0°$), based on our own NMR findings of a type I β-turn spanning residues Pro6-Asp7-Thr8-Arg9 (see Results). Pro6, Arg9, Pro10, Ala11, Pro12, Gly13, Ser14, Thr15, and Ala16 were set to a polyproline type II helical conformation ($\phi = -60°$, $\psi = 70°$), based on Fontenot's findings of a significant population of polyproline type II helix in his CD studies of multiple repeat MUC1 peptides (*47*−*49*).

(2) The ϕ and ψ dihedral angles of Thr3, Ser4, and Ala5 were then manually rotated to bring the Tn3 and Tn4 carbohydrates to the same face of the glycopeptide as the side chain of Thr8. The modeling of an antibody binding interface involving Tn3, Tn4, and Thr8 is based on the observation of Fab NOEs to Tn3, Tn4, and Thr8 in the 5 and 25 °C TRNOESY spectra of the Tn3,Tn4-glycosylated MUC1 16mer peptide in the presence of Fab B27.29 (see Results and Table S6).

(3) Finally, 5000 iterations of conjugate gradient energy minimization in vacuo using a distance-dependent dielectric and a CVFF force field were performed. Peptide−sugar distance restraints observed for the Fab-bound peptide were used throughout the minimization to establish the "correct", experimentally observed orientation of the Tn sugar groups relative to the peptide backbone. Distance restraints were calculated from the peptide−sugar NOEs observed in the 25 °C TRNOESY spectrum of the Tn3,Tn4-glycosylated MUC1 16mer peptide in the presence of Fab B27.29 (see Table S8). Only peptide−sugar NOEs observed at 25 °C (not at 5 °C) were used for distance restraints in order to minimize the contribution of the "free" peptide−sugar NOEs to the measured intensities. NOE intensities were measured as integral volumes and were converted to distance restraints using the following classifications: strong (1.8 Å $\leq r_{ij} \leq$ 3.5 Å), medium (1.8 Å $\leq r_{ij} \leq$ 5.0 Å), and weak (3.5 Å $\leq r_{ij} \leq$ 6.0 Å). Distance information was included using a flat-bottomed potential which was equal for all restraints. All peptide bonds were forced to trans geometry during the calculations. No distance violations greater than 0.1 Å were observed in the final energy-minimized structure.

RESULTS

Chemical Shifts and Resonance Assignments for the Unglycosylated and Tn-Glycosylated MUC1 16mers. Table

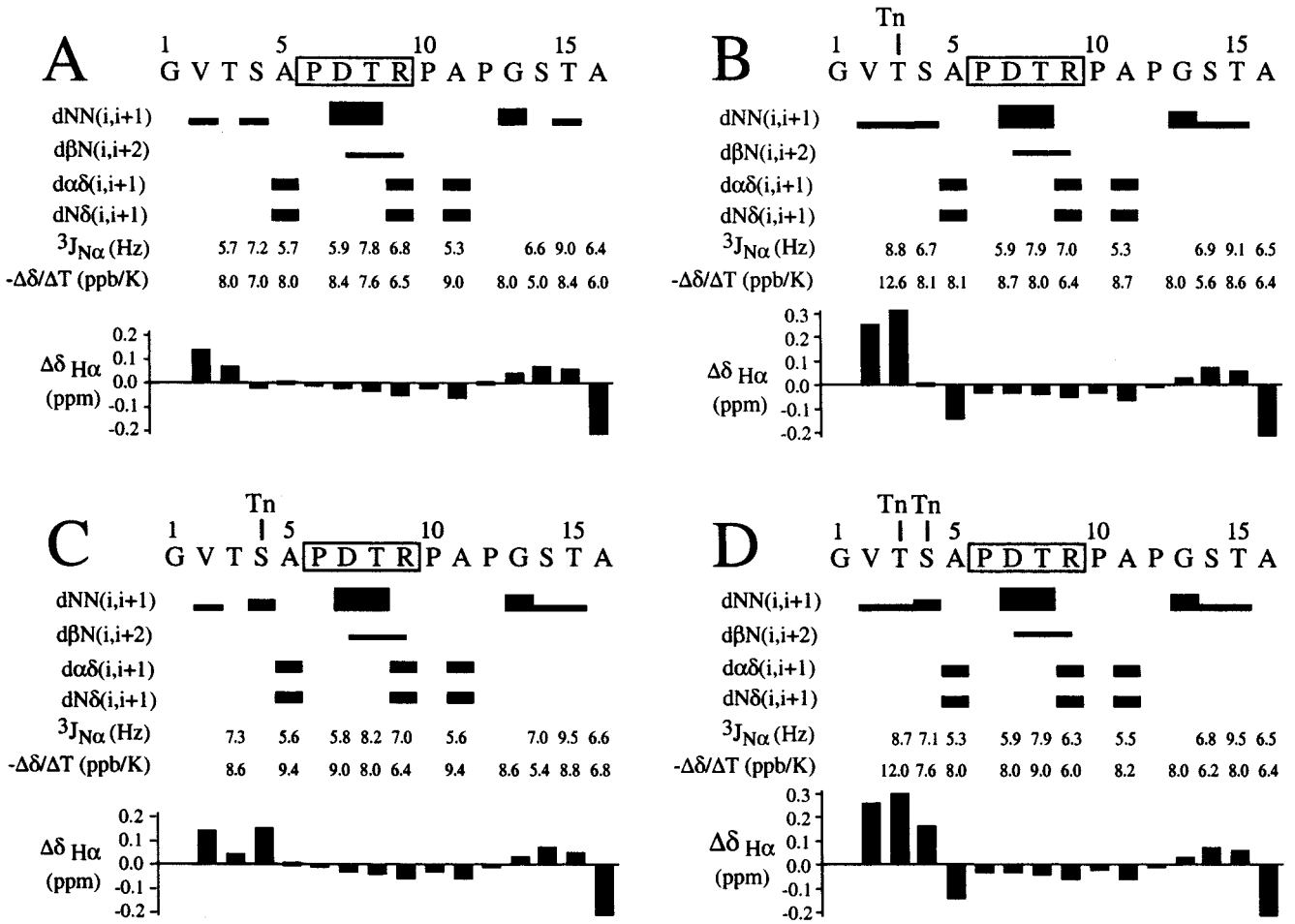

FIGURE 1: Schematic diagram showing the magnitude of *d*NN, *dβ*N, *dαδ*, and *dNδ* NOE connectivities observed in the NOESY spectrum of the unglycosylated MUC1 16mer (panel A), Tn3-glycosylated MUC1 16mer (panel B), Tn4-glycosylated MUC1 16mer (panel C), and Tn3,Tn4-glycosylated MUC1 16mer (panel D). The diagram also includes coupling constants ($^3J_{N\alpha}$), temperature coefficients ($-\Delta\delta/\Delta T$), and chemical shift deviations ($\Delta\delta_{H\alpha} = \delta_{H\alpha}$obs $- \delta_{H\alpha}$coil). Uncertainty in the measured temperature coefficient values is ±0.2 ppb/K. Uncertainty in the measured coupling constants is ±0.2 Hz. The strong sequential *d*NN(*i*,*i*+1) NOEs between Asp7 and Thr8 and between Thr8 and Arg9, and the medium *dβ*N(*i*,*i*+2) NOE between Asp7 and Arg9 define a type I *β*-turn spanning Pro6-Asp7-Thr8-Arg9 in each peptide (boxed). The medium *dαδ*(*i*,*i*+1) and *dNδ*(*i*,*i*+1) NOEs linking all X-Pro pairs in the sequence define an all-trans configuration (*53*) for each peptide.

S1 (in Supporting Information) presents the ^{1}H NMR assignments for the peptide and carbohydrate resonances of the unglycosylated, Tn3-glycosylated, Tn4-glycosylated, and Tn3,Tn4-glycosylated MUC1 16mers in 90% H_2O/10% D_2O PBS buffer, pH 7.0, 5 °C. Table S2 presents the ^{13}C NMR assignments for the unglycosylated and Tn3,Tn4-glycosylated 16mers in 99.9% D_2O PBS buffer, pH 7.0, 5 °C, obtained from natural abundance ^{13}C-edited HSQC spectra. With allowances made for different temperature and solvent conditions, assignments are in good agreement with those previously published in 60% CD_3OH/40% H_2O, pH 5.5, 10 °C (*50*).

The assignments in Tables S1 and S2 show that glycosylation-induced chemical shift perturbations are localized to residues at or immediately adjacent to the site of carbohydrate attachment. For example, a comparison of the chemical shifts for the unglycosylated 16mer versus the Tn4-glycosylated 16mer shows significant downfield shifts for the NH and Hα resonances of Ser4 (8.49−8.71 and 4.45−4.62 ppm, respectively), less significant shifts for the NH of Ala5 (8.53−8.65 ppm), and only small perturbations for the Hα and H*β* resonances of Thr3. Even the doubly glycosylated 16mer exhibits no significant ^{1}H or ^{13}C chemical shift perturbations for residues more than two positions removed from the site(s) of carbohydrate attachment. Indeed, the chemical shifts for the backbone and side chain resonances of residues within the PDTRP peptide epitope region are virtually identical across the series of MUC1 16mer peptides and glycopeptides studied (see Table S1), suggesting that the chemical environment of the peptide epitope region is unaffected by upstream glycosylation events at Thr3 and Ser4.

The localized glycosylation-induced chemical shift perturbations observed in Tables S1 and S2 can be correlated to localized shifts in the conformational equilibrium of the underlying peptide backbone, as assessed from a calculation of the deviation of the ^{1}Hα proton and ^{13}Cα carbon chemical shift values from random coil (*51*). $\Delta\delta_{H\alpha}$ and $\Delta\delta_{C\alpha}$ values (observe − random coil) were calculated for the unglycosylated and Tn-glycosylated MUC1 16mer peptides, and these values are presented in Table S3 and panels A (unglycosylated 16mer), B (Tn3-glycosylated 16mer), C (Tn4-glycosylated 16mer), and D (Tn3,Tn4-glycosylated 16mer) of Figure 1. The $\Delta\delta_{H\alpha}$ and $\Delta\delta_{C\alpha}$ values for the unglycosylated 16mer are close to random coil (*52*) for all residues, excepting Gly1 and Val2 at the N-terminus and

Ala16 at the C-terminus. In contrast, the $\Delta\delta_{H\alpha}$ and $\Delta\delta_{C\alpha}$ values for glycosylated residues in the Tn-glycosylated 16mers show significant downfield shifts and upfield shifts, respectively. These values are consistent with an increase in the population of extended structure for these residues[3] and suggest that glycosylation shifts the conformational equilibrium of the underlying peptide backbone toward the extended strand. This phenomenon probably arises from limitations placed by the carbohydrate on the ϕ, ψ dihedral space available to the underlying peptide backbone. In line with these steric arguments is the observation that Tn-glycosylation at either Thr3 or Ser4 shifts the degenerate Hβ resonances of Ser4 (3.85 ppm for the unglycosylated 16mer) into nondegenerate positions (3.76 and 3.91 ppm in the Tn4-glycosylated 16mer, for example), which suggests that carbohydrate also hinders rotation about the χ_1 bond of Ser4.

NOESY Connectivities for the Unglycosylated and Tn-Glycosylated MUC1 16mers. The NOEs diagnostic of β-turn secondary structure include *d*NN(2,3), *d*NN(3,4), and *d*αN(2,4) cross-peaks (*53*), where the numbering indicates the position in the turn. Figure 1 shows the magnitudes of these β-turn-defining NOEs observed in the NOESY spectra of the unglycosylated (panel A), Tn3-glycosylated (panel B), Tn4-glycosylated (panel C), and Tn3,Tn4-glycosylated (panel D) 16mer peptides. All peptides display strong sequential *d*NN(*i*,*i*+1) NOEs between Asp7 and Thr8 and between Thr8 and Arg9. These NOEs are diagnostic of a type I β-turn ($\phi_2 = -60°$, $\psi_2 = -30°$, $\phi_3 = -90°$, $\psi_3 = 0°$) spanning Pro6-Asp7-Thr8-Arg9 within the PDTRP peptide epitope region of each peptide, as such a turn would give rise to equally strong *d*NN(2,3) and *d*NN(3,4) NOEs (*54*). A type I β-turn conformation for this region in each peptide is further suggested by the medium *d*βN(2,4) NOEs observed between Asp7 and Arg9, since this distance can approach as closely as 2.9 Å in a type I turn but only as closely as 3.6 Å in a type II turn[4] (*54*). Glycosylation does not appear to affect either the stability or conformation of the type I β-turn, as the relative intensities of the *d*NN(2,3) and *d*NN(3,4) NOEs measured in the unglycosylated versus Tn-glycosylated 16mer NOESY spectra are comparable. This suggests that the conformation of the peptide PDTRP epitope region is unaffected by upstream glycosylation events at Thr3 and Ser4.

Our findings of a type I β-turn spanning the PDTR sequences of the unglycosylated and Tn-glycosylated MUC1 16mer peptides are in agreement with the results of three separate biophysical studies of MUC1 peptides: the previously referenced NMR study involving the unglycosylated and Tn3,Tn4-glycosylated 16mer peptides in methanol/water (*50*), an earlier NMR study by another group involving a 20-residue MUC1 peptide (PDTRPAPGSTAPPAHGVTSA) in DMSO (*55*), and our own recent NMR studies involving a shorter 9-residue MUC1 peptide (TSAPDTRPA) in water (*31*). Other studies of MUC1 peptides have found different favored turn conformations for the PDTR sequence. Fontenot and co-workers proposed a type II β-turn conformation ($\phi_2 = -60°$, $\psi_2 = +120°$, $\phi_3 = +90°$, $\psi_3 = 0°$) on the basis of their NMR/CD studies of three-repeat MUC1 peptides in water (*47*−*49*). However, a type II conformation would give rise to a weak *d*NN(2,3) cross-peak between Asp7 and Thr8, which is not observed in our 16mer peptides. It has also been proposed by Kirnarsky and co-workers on the basis of their NMR structure calculations that the PDTR sequence adopts two overlapping inverse γ-turns in solution, the first spanning Pro-Asp-Thr and second Asp-Thr-Arg (*56*). However, the strong *d*NN(*i*,*i*+1) connectivities observed for this region of the sequence argue against the existence of two overlapping inverse γ-turns, as this arrangement would give rise to only weak *d*NN(*i*,*i*+1) cross-peaks between Asp7 and Thr8 and between Thr8 and Arg9, corresponding to distances of 3.8 Å in each γ-turn.[5] Although it is conceivable that the different experimental conditions used in each NMR study might have led to a different favored turn conformation, it is more probable that the PDTR region of the MUC1 epitope is conformationally heterogeneous, sampling different turn conformations (type I β-turn, type II β-turn, inverse γ-turn, etc.) as part of a complex conformational equilibrium. This possibility has been explored in greater detail in our recently published NMR studies of a 9-residue MUC1 peptide and its Tn-glycosylated derivative (*31*).

Coupling Constants for the Unglycosylated and Tn-Glycosylated MUC1 16mers. Type I and type II β-turns are characterized by a dihedral angle of $\phi_2 = -60°$ for the second residue in the four-residue turn (*57*, *58*). This local conformation is consistent with a coupling constant of 4 Hz $\leq {}^3J_{N\alpha} \leq$ 5 Hz, assuming a β-turn which is stably folded (100% populated) in solution. ${}^3J_{N\alpha}$ coupling constants were measured for all non-proline and non-glycine residues in the unglycosylated and Tn-glycosylated MUC1 16mer peptides, and these values are presented in Table S3 and panels A (unglycosylated 16mer), B (Tn3-glycosylated 16mer), C (Tn4-glycosylated 16mer), and D (Tn3,Tn4-glycosylated 16mer) of Figure 1. All peptides display reduced coupling constants for Ala5 and Ala11, a result of their placement prior to a proline (Pro6 and Pro12) in the MUC1 sequence.[6] All peptides also display a reduced coupling constant for Asp7 in position 2 of the putative type I β-turn, which is the same value within error (5.9 ± 0.1 Hz) across the series of 16mer peptides and glycopeptides. This value does not fall within the range of 4 Hz $\leq {}^3J_{N\alpha} \leq$ 5 Hz predicted for the second residue of a stably folded type I β-turn. However,

[3] Hα proton chemical shift deviations measured for all 20 naturally occurring amino acids show a mean α proton shift of −0.39 ppm (upfield from the random coil value) when the residue is placed in a helical conformation and a mean α proton shift of +0.37 ppm when the residue is placed in an extended conformation (*51*). The shifting tendancies for ^{13}C nuclei are opposite in direction to those found for ^{1}NH and ^{1}Hα protons, so that the ^{13}Cα carbons experience a upfield shift from the random coil value when in an extended conformation (*51*).

[4] Unfortunately, the *d*αN(2,4) NOE between Asp7 and Arg9 is overlapped with the intraresidue *d*αN of Arg9 in the NOESY spectrum of each MUC1 16mer peptide (the Hα resonances of Arg7 and Arg9 are degenerate in each case). However, this NOE has been observed in the NOESY spectra of both the unglycosylated and Tn3,Tn4-glycosylated 16mer peptides in a methanol/water mixture (*50*).

[5] The NOEs characteristic of an inverse γ-turn ($-85° \leq \phi 2 \leq -70°$, $+60° \leq \psi 2 \leq +70°$) (*57*, *58*) include a strong *d*αN(2,3) cross-peak, corresponding to a distance of 2.4 Å, a weak *d*NN(2,3) cross-peak, corresponding to a distance of 3.8 Å, and a weak *d*αN(1,3) cross-peak corresponding to a distance of 4.3 Å (*59*, *60*).

[6] In general, a residue proceeding a proline experiences steric clashes between its NH, Hα, and Hβ protons and the Hδ protons and carbonyl carbons of the proline. This results in a displacement toward more negative ϕ values for the proceeding residue and a concomitant decrease in the measured ${}^3J_{N\alpha}$ value (*61*).

as the partially structured 16mer peptides and glycopeptides are likely to be undergoing a conformational equilibrium between folded (β-turn) and unfolded (extended) states, the measured coupling constants for Asp7 should represent a populated weighted average of the $^3J_{\alpha N}$ values associated with each interconverting state. Using a two-state model (*62*, *63*) in which Asp7 can find itself either in a turn conformation ($^3J_{N\alpha} = 5$ Hz) or in an extended conformation ($^3J_{N\alpha} = 9$ Hz), a measured coupling constant of $^3J_{N\alpha} = 5.9 \pm 0.1$ Hz translates into approximately 70−75% of Asp7 sites in a folded turn conformation for each peptide. This rough estimate suggests that the turn population within the PDTRP epitope region is unaffected by upstream glycosylation events at Thr3 and Ser4, in agreement with the NOE and chemical shift perturbation data previously discussed.

Whereas the coupling constant data suggest no long-range effects of glycosylation, the dependence of the $^3J_{N\alpha}$ of Thr3 on the glycosylation state suggests significant localized effects. For example, the $^3J_{N\alpha}$ of Thr3 increases from 5.7 Hz in the unglycosylated 16mer, to 7.3 Hz in the Tn4-glycosylated 16mer, to 8.8 Hz in the Tn3-glycosylated 16mer. Using the simple but conceptually effective two-state model described above, these coupling constants translate into approximately 17%, 58%, and 95% local extended conformation, respectively, for each peptide. These rough estimates suggest that glycosylation shifts the conformational equilibrium of the underlying peptide backbone toward extended strand, a finding consistent with the chemical shift data presented earlier in the paper.

Temperature Coefficients for the Unglycosylated and Tn-Glycosylated MUC1 16mers. The temperature dependence of the amide proton chemical shift, or temperature coefficient ($-\Delta\delta/\Delta T$), is often interpreted as a measure of solvent shielding in folded peptides and proteins. For unfolded regions of the sequence, temperature coefficients are expected to be $6 \leq -\Delta\delta/\Delta T \leq 10$ ppb/K (*64*), indicating that the backbone is freely solvated by water and that no hydrogen bonds are present which would protect the backbone amides from solvent exchange. For folded regions of the sequence, temperature coefficients are expected to decrease to $-\Delta\delta/\Delta T < 6$ ppb/K (*64*), indicating either the presence of a hydrogen bond or a high degree of solvent shielding. The temperature dependence of the amide proton chemical shift can therefore be an indication of possible intramolecular hydrogen bonding.

Temperature coefficients ($-\Delta\delta/\Delta T$) were measured for all non-proline residues in the unglycosylated and Tn-glycosylated MUC1 16mer peptides, and these values are presented in Table S3 and panels A (unglycosylated 16mer), B (Tn3-glycosylated 16mer), C (Tn4-glycosylated 16mer), and D (Tn3,Tn4-glycosylated 16mer) of Figure 1. All peptides display reduced temperature coefficients of $6.0 \leq -\Delta\delta/\Delta T \leq 6.5$ ppb/K for Arg9 in position 4 of the putative type I β-turn. These reduced temperature coefficients suggest involvement of the Arg9 NH in a hydrogen bond that partially protects it from solvent exchange, an interpretation consistent with the presence of Pro6−CO to Arg9−NH (1,4) hydrogen bonds stabilizing the type I β-turn proposed to span Pro6-Asp7-Thr8-Arg9 within the PDTRP peptide epitope region of each peptide.

Also observed in the temperature coefficient data is an unusually strong dependence of the $-\Delta\delta/\Delta T$ of Thr3 on the glycosylation state of this residue. For example, the $-\Delta\delta/\Delta T$ of Thr3 is much more elevated in the Tn3- and Tn3,Tn4-glycosylated 16mers (12.6 and 12.0 ppb/K, respectively) than in the unglycosylated or Tn4-glycosylated 16mers (8.0 and 8.6 ppb/K, respectively). These elevated values of $-\Delta\delta/\Delta T$ correlate with the significant downfield shifts observed for Thr3 NH in the Tn3- and Tn3,Tn4-glycosylated 16mers (8.91 and 8.90 ppm, respectively), in agreement with the strong correlation that exists between $-\Delta\delta/\Delta T$ and NH chemical shift in unstructured systems (*65*). One way to interpret the significant downfield shifts of Thr3 NH in the Tn3-glycosylated and Tn3,Tn4-glycosylated 16mers is to relate it to the possible existence of a hydrogen bond between the backbone NH proton of Thr3 and the carbonyl of the *N*-acetyl group of Tn3,[7] as the presence of hydrogen bonds is often accompanied by marked downfield shifts in folded peptides and proteins (*65*). This proposal receives some support from molecular modeling studies of a glycosylated trimer Ac-Thr(α-GalNAc)-Ala-Ala-OMe (*66*) in which the existence of a hydrogen bond between the peptide NH protons and

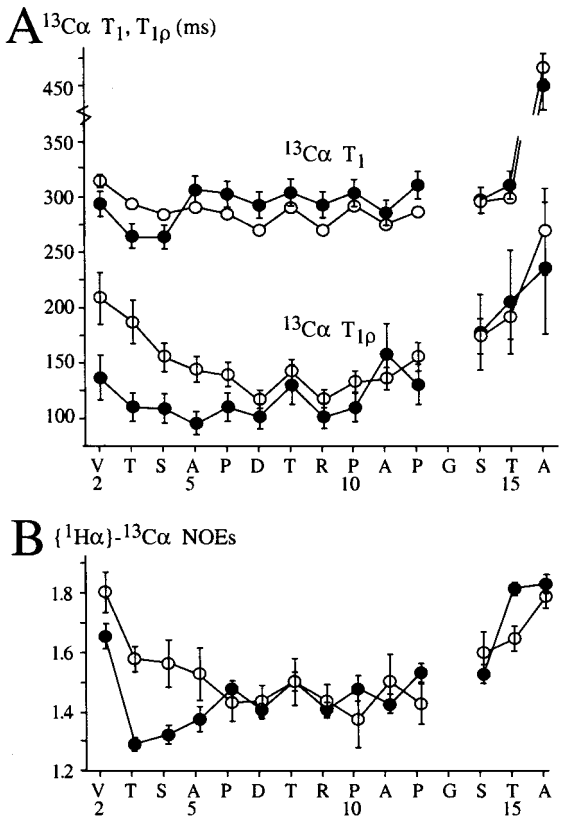

FIGURE 2: Natural abundance ^{13}Cα relaxation data measured for the unglycosylated (open circles) and Tn3,Tn4-glycosylated (black circles) MUC1 16mer peptides. Panel A plots the ^{13}Cα T_1 and $T_{1\rho}$ relaxation times, and panel B plots the {^{1}Hα}−^{13}Cα heteronuclear NOE values measured for each residue. Error bars (standard deviations calculated for each relaxation parameter) are plotted only when the bars are larger than the actual size of the symbol. Experimental conditions were 10 mM peptide in 99.9% D_2O PBS buffer, pH 7.0, 5 °C.

[7] It should be noted that the proposal of a hydrogen bond based on large negative values of $-\Delta\delta/\Delta T$ is consistent with the "equilibrium between states" interpretation of temperature coefficients (*65*), although it does contradict the conventional "solvent shielding" interpretation of $-\Delta\delta/\Delta T$ (*64*) which assumes a correlation between small $-\Delta\delta/\Delta T$ and the presence of a hydrogen bond.

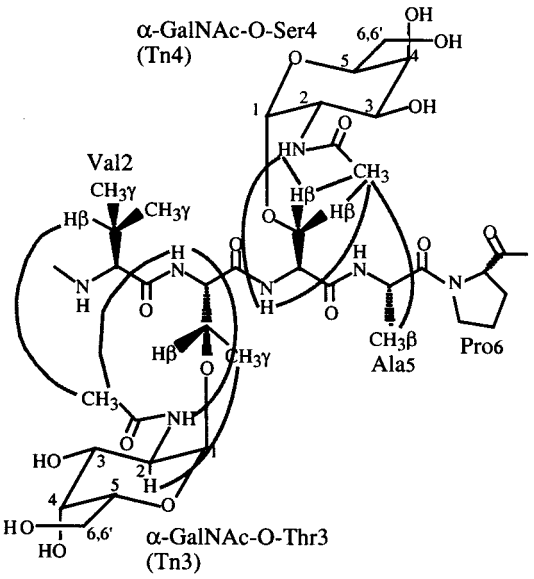

FIGURE 3: Diagrammatic representation of strong peptide−sugar NOEs observed in the NOESY spectrum of the Tn3,Tn4-glycosylated MUC1 16mer peptide acquired in 90% H_2O/10% D_2O PBS buffer, pH 7.0, 5 °C. Refer to Table S5 for a complete list of peptide−sugar NOEs.

the GalNAc *N*-acetyl carbonyl was demonstrated. Were such hydrogen bonds to exist in the Tn-glycosylated MUC1 16mers, these bonds might also play a role in shifting the conformation of the underlying peptide backbone toward more extended structure.

^{13}C NMR Relaxation Experiments for the Unglycosylated and Tn3,Tn4-Glycosylated MUC1 16mers. Natural abundance ^{13}Cα T_1 and $T_{1\rho}$ relaxation times and {^{1}Hα}−^{13}Cα heteronuclear NOE values were measured for the unglycosylated and Tn3,Tn4-glycosylated MUC1 16mer peptides in order to assess the effect of carbohydrate attachment at Thr3 and Ser4 on peptide backbone dynamics. The relaxation times and NOE values presented in Table S4 and panels A (^{13}Cα T_1 and $T_{1\rho}$) and B ({^{1}Hα}−^{13}Cα NOE) of Figure 2 show that glycosylation significantly affects the backbone dynamics of glycosylated (Thr3, Ser4) and neighboring (Val2, Ala5) residues but has no significant effects on the backbone dynamics of more remote residues within the PDTRP core epitope region. For example, the relaxation times and NOE values of Thr3 are $T_1 = 295 \pm 5$ ms, $T_{1\rho} = 188 \pm 19$ ms, and NOE $= 1.58 \pm 0.04$ for the unglycosylated 16mer and $T_1 = 262 \pm 11$ ms, $T_1\rho = 110 \pm 13$ ms, and NOE $= 1.29 \pm 0.02$ for the Tn3,Tn4-glycosylated 16mer. These times and values are consistent with glycosylation-induced increases in the local correlation time and order of the Thr3 ^{13}Cα−^{1}Hα bond vector. In contrast, the relaxation times and NOE values averaged over the central residues of the peptide (Pro6-Asp7-Thr8-Arg9-Pro10-Ala11-Pro12) are not significantly changed by upstream glycosylation at Thr3 and Ser4; i.e., $\langle T_1\rangle_{6-12} = 281 \pm 9$ ms, $\langle T_{1\rho}\rangle_{6-12} = 134 \pm 21$ ms, and $\langle \text{NOE}\rangle_{6-12} = 1.44 \pm 0.05$ for the unglycosylated 16mer and $\langle T_1\rangle_{6-12} = 298 \pm 9$ ms, $\langle T_{1\rho}\rangle_{6-12} = 120 \pm 21$ ms, and $\langle \text{NOE}\rangle_{6-12} = 1.46 \pm 0.05$ for the Tn3,Tn4-glycosylated 16mer. Our findings of only localized effects of glycosylation on underlying peptide backbone dynamics are in agreement with the ^{13}C NMR relaxation studies of a sequentially deglycosylated native ovine submaxillary mucin (OSM) (*67*), where a "stiffening effect" was found to be

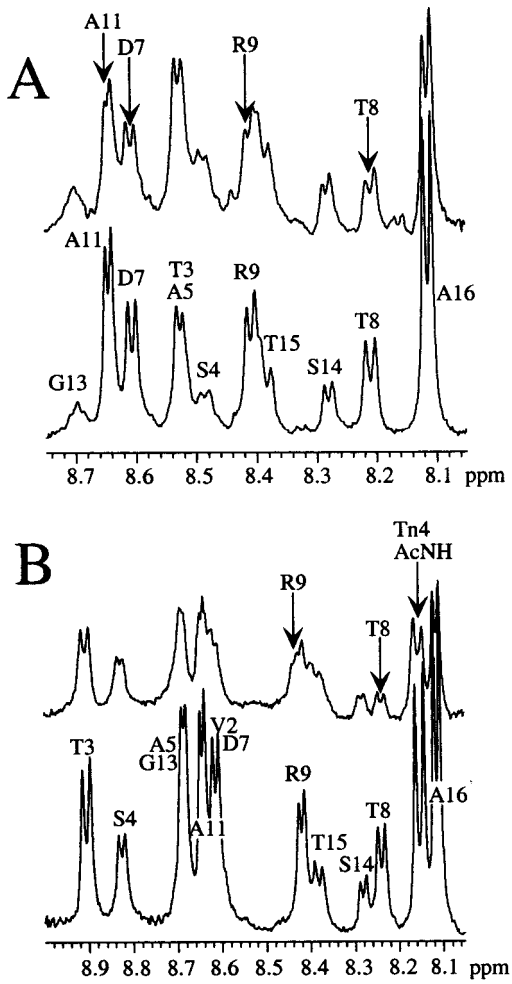

FIGURE 4: Backbone amide NH regions of ^{1}H NMR spectra showing the forward titration of the unglycosylated (panel A) and Tn3,Tn4-glycosylated (panel B) MUC1 16mer peptides with Fab B27.29. The lower traces correspond to the free peptides, whereas the upper traces correspond to the peptide in the presence of 0.4 molar equiv of Fab. Resonances marked by arrows experience the greatest losses in signal intensity due to line broadening in the presence of Fab. Experimental conditions were 1 mM peptide ± 400 μM Fab in 90% H_2O/10% D_2O PBS buffer, pH 7.0, 5 °C.

transmitted from the site of glycosylation only to adjacent nonglycosylated residues.

Peptide−Sugar NOE Connectivities Identified for the Tn3,Tn4-Glycosylated MUC1 16mer. The ^{13}C NMR relaxation results described above suggest that glycosylation exerts its conformational effects on the underlying mucin peptide backbone through the imposition of steric constraints on ϕ,ψ dihedral space. However, a second mechanism involving conformational effects through specific peptide−sugar interactions is also possible. To probe for the existence of specific peptide−sugar interactions that could mediate conformational effects on local peptide backbone, NOESY spectra of the Tn3,Tn4-glycosylated MUC1 16mer peptide were carefully scrutinized for peptide−sugar NOEs. These NOEs, listed in Table S5 and shown diagramatically in Figure 3, suggest that interactions between the attached sugar and the underlying peptide backbone are specific and localized. For example, the Tn3 carbohydrate displays close contacts only to Val2, Thr3, and Ser4, whereas the Tn4 carbohydrate displays close contacts only to Ser4, Ala5, and Pro6. The absence of longer range contacts between the

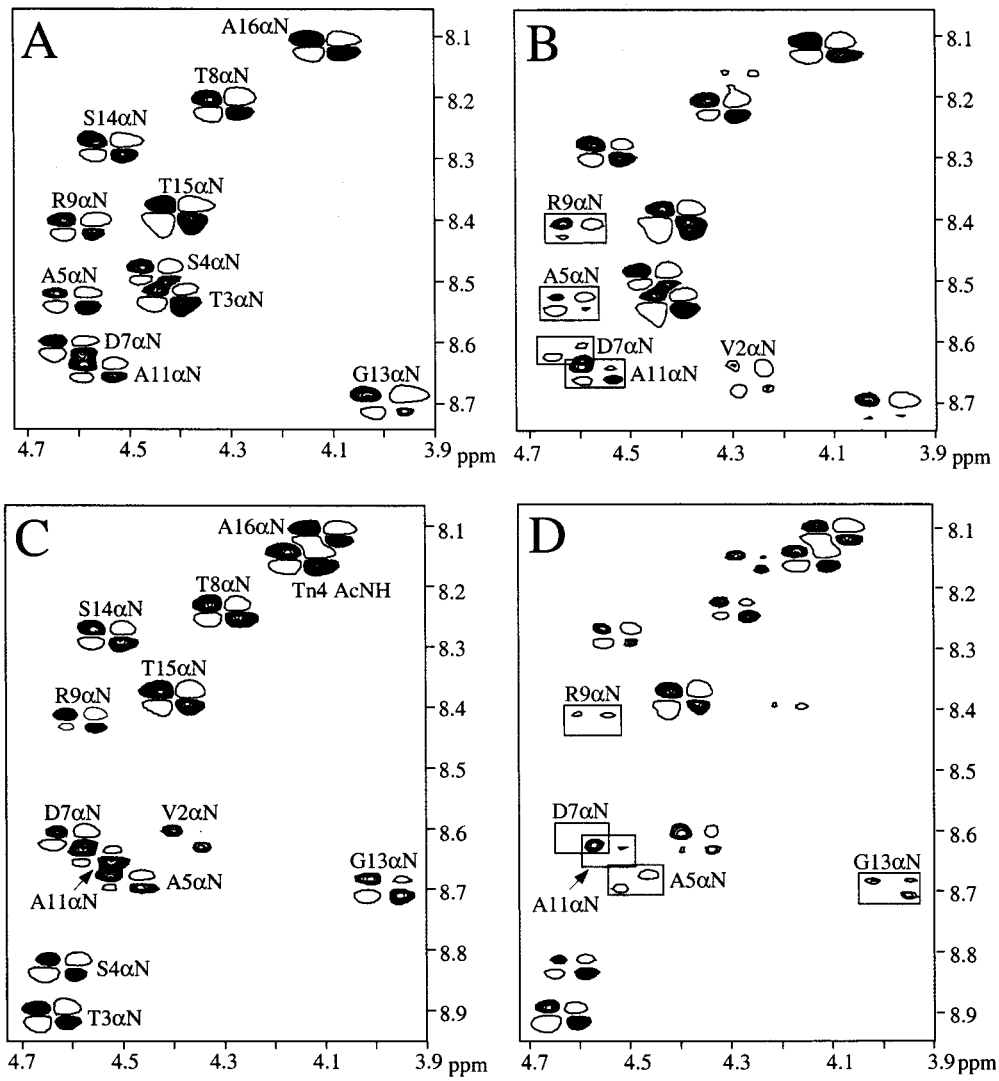

FIGURE 5: Fingerprint *d*αN regions of DQFCOSY spectra showing the forward titration of the unglycosylated and Tn3,Tn4-glycosylated MUC1 16mers with Fab B27.29. Panels A and B correspond to the unglycosylated 16mer in the absence (panel A) and presence (panel B) of 0.4 molar equiv of Fab, whereas panels C and D correspond to the Tn3,Tn4-glycosylated 16mer in the absence (panel C) and presence (panel D) of 0.4 molar equiv of Fab. Boxed cross-peaks experience the greatest losses in signal intensity due to line broadening in the presence of Fab. Experimental conditions were 1 mM peptide ± 400 μM Fab in 90% H_2O/10% D_2O PBS buffer, pH 7.0, 5 °C.

attached Tn carbohydrates and the peptide backbone is consistent with the absence of longer range effects on the conformation or dynamics of the peptide PDTRP epitope region following upstream glycosylation at either Thr3 or Ser4.

Some of the strongest NOEs observed in the NOESY spectra of the Tn3,Tn4-glycosylated MUC1 16mer peptide include those between the NH protons of Thr3 and Ser4 and the methyl and NH protons of the *N*-acetyl groups of their directly attached Tn moieties. Similar peptide−sugar connectivities have been observed in other NMR studies of α-GalNAc O-glycosylated peptides (*31*, *56*, *68*, *69*). For example, Kirnarsky and co-workers observed a strong NOE between the NH proton of their glycosylated threonine residue and the *N*-acetyl group of GalNAc in their α-linked O-glycosylated 15-residue MUC1 peptide (*56*). The presence of these specific peptide−sugar NOEs between the *N*-acetyl group of the attached GalNAc and the backbone NH of the glycosylated residue suggests that the *N*-acetyl of the GalNAc might interact directly with the peptide backbone, providing some evidence for the existence of hydrogen bonds between the NH proton of the peptide backbone and the carbonyl on the *N*-acetyl group of the GalNAc. However, it is not clear from the pattern of peptide−sugar NOEs why such a hydrogen bond should be stronger for the Thr3−Tn3 pair than for the Ser4−Tn4 pair, as suggested by the temperature coefficient data.

^{1}H NMR-Monitored Titrations of the Unglycosylated and Tn3,Tn4-Glycosylated MUC1 16mers with Fab 27.29. Competitive ELISA binding studies on mucin solid phase have shown that Tn glycosylation at Thr3 and Ser4 in the MUC1 synthetic peptides leads to a small but reproducible increase in the affinity of the peptide for Mab B27.29, an antibody raised against the intact tumor-associated MUC1 mucin (*50*). As upstream glycosylation at Thr3 and Ser4 does not affect the conformation and dynamics of the immunodominant PDTRP peptide epitope region, this increased affinity for B27.29 cannot be due to the proximal carbohydrate stabilizing the peptide epitope conformation most favored for binding (presumably the type I β-turn spanning PDTR). A more likely scenario is that the carbohydrates comprise part of the recognition domain for B27.29, whose natural MUC1

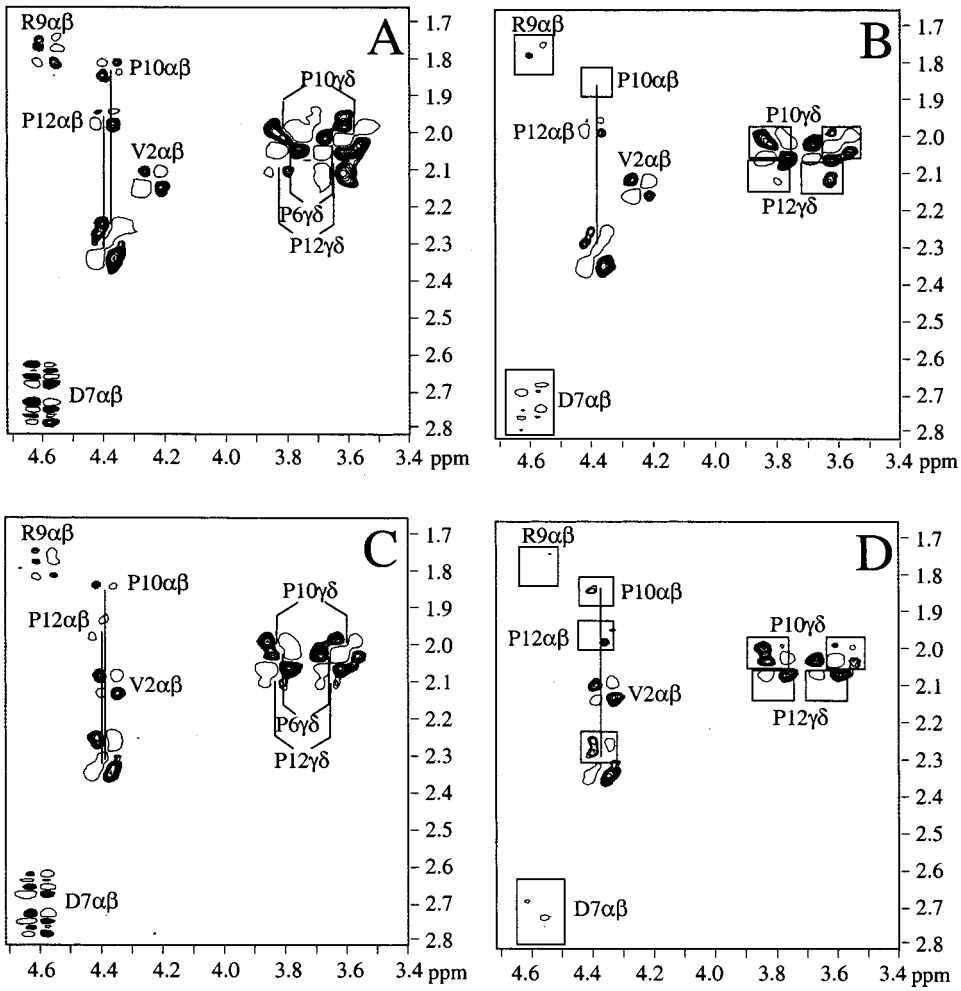

FIGURE 6: Aliphatic regions of DQFCOSY spectra showing the forward titration of the unglycosylated and Tn3,Tn4-glycosylated MUC1 16mers with Fab B27.29. Panels A and B correspond to the unglycosylated 16mer in the absence (panel A) and presence (panel B) of 0.4 molar equiv of Fab, whereas panels C and D correspond to the Tn3,Tn4-glycosylated 16mer in the absence (panel C) and presence (panel D) of 0.4 molar equiv of Fab. Boxed cross-peaks experience the greatest losses in signal intensity due to line broadening in the presence of Fab. Experimental conditions were 1 mM peptide ± 400 μM Fab in 90% H_2O/10% D_2O PBS buffer, pH 7.0, 5 °C.

antigen remains extensively glycosylated with cryptic carbohydrate structures in the tumor-associated state.

To determine the contribution of defined peptide secondary structure (peptide epitope) versus specific-site glycosylation (carbohydrate epitope) in antibody recognition and binding, ^{1}H NMR-monitored titrations of the unglycosylated and Tn3,Tn4-glycosylated MUC1 16mers with the Fab fragment of Mab B27.29 were performed. Figure 4 shows the backbone amide region of the 500 MHz ^{1}H NMR spectra of the unglycosylated 16mer (panel A) and Tn3,Tn4-glycosylated 16mer (panel B) in the absence and presence of 0.4 molar equiv of Fab B27.29. Several amide resonances are observed to diminish appreciably in the bound spectrum, due to exchange broadening and/or increases in local correlation time as these residues are preferentially bound and immobilized in the antibody combining site. The spectrum of the glycosylated 16mer shows greater line broadening effects than does the spectrum of the unglycosylated 16mer at the same molar equivalents of Fab. This suggests a stronger interaction for the glycosylated peptide, in agreement with the competitive ELISA binding experiments (*50*). Regardless of these differences in overall line broadening, the most selectively broadened amide resonances for each peptide correspond to Asp7, Thr8, Arg9, and Ala11 within or near the PDTR β-turn region. This collection of residues suggests that the turn is preferentially bound in the antibody combining site and constitutes the peptide portion of the B-cell epitope for both the unglycosylated 16mer and the Tn3,Tn4-glycosylated 16mer. The sugar moieties must also be involved in the binding of Fab, since the *N*-acetyl NH resonance(s) of Tn3 (not shown) and Tn4 are observed to substantially diminish in intensity in the bound spectra of the glycosylated 16mer.

The identification of epitope regions using differential line broadening is best accomplished using the DQFCOSY experiment, as the antiphase nature of the cross-peaks renders them uniquely sensitive to the line width of the detected proton (the positive and negative lobes cancel once line width exceeds coupling). Thus, the DQFCOSY experiment can act as a dynamic filter of differential proton mobilities and has been used in this capacity to identify the residues comprising the determinants of several peptide antigens when these are bound to antibody (70−72). Figure 5 shows the $d_{\alpha N}$ fingerprint regions of the 500 MHz DQFCOSY spectra of the unglycosylated and Tn3,Tn4-glycosylated 16mer peptides in the absence (panel A) and presence (panel B) of Fab B27.29, where several $d_{\alpha N}$ cross-peaks are observed to disappear or diminish appreciably in intensity upon the

addition of antibody. Those $d_{\alpha N}$ cross-peaks correspond to Ala5, Asp7, Arg9, and Ala11 in each peptide, residues within or near the PDTR β-turn region. However, the backbone (as detected by the $d_{\alpha N}$ cross-peak) is not the only portion of the turn that is selectively immobilized upon binding to antibody. When the $d_{\alpha\beta}$ regions of the DQFCOSY experiments are plotted for each peptide in the absence and presence of Fab (see panels A and B of Figure 6), the $d_{\alpha\beta}$ cross-peaks which experience the greatest line broadening correspond to the β protons of Asp7, Arg9, and Pro10 in each peptide, suggesting that the side chains of these residues are also partially immobilized in the antibody combining site. Thus, the side chains as well as the backbone portion of the PDTRP peptide epitope appear to be involved in the recognition and binding of Fab B27.29.

TRNOESY Studies of the Binding of the Tn3,Tn4-Glycosylated MUC1 16mer to Fab 27.29. TRNOESY experiments were next performed at both 5 and 25 °C for the Tn3,Tn4-glycosylated 16mer peptide in the presence of Fab B27.29. The goals of these TRNOESY experiments were threefold: (1) to map the MUC1 B-cell epitope recognized by B27.29, (2) to identify peptide−Fab and sugar−Fab NOEs across the binding interface so as to better define the MUC1 antigen−B27.29 interaction, and (3) to determine if the PDTR type I β-turn found within the free solution state MUC1 peptide is conserved within the B27.29 combining site.

Figure 7 shows the $d\alpha$N, $d\beta$N, $d\gamma$N, and $d\delta$N regions of the NOESY and TRNOESY spectra acquired at 25 °C from the reverse titration of the Tn3,Tn4-glycosylated 16mer in the absence (panel A) and the presence (panel B) of Fab B27.29. This figure illustrates the development of TRNOEs in the bound glycopeptide, which are more easily observed at 25 °C due to the attenuation of the free peptide NOEs at this temperature. The strongest of these TRNOEs correspond to residues within the PDTRP epitope. For example, the $d\beta$N and $d\gamma$N cross-peaks of Asp7, Thr8, and Arg9 are observed only in the presence of Fab (Figure 7B). TRNOE effects are also observed for the Tn-glycosylated residues Thr3 and Ser4 and for the Tn carbohydrates attached to these residues. No TRNOE effects are observed for the C-terminal residues of the glycopeptide, as evidenced by the absence of $d\alpha$N, $d\beta$N, and $d\gamma$N cross-peaks for Gly13, Ser14, Thr15, and Ala16 in the presence of Fab (Figure 7B). The aliphatic portion of the TRNOESY spectrum of the Tn3,Tn4-glycosylated 16mer in the presence of Fab B27.29 was also analyzed (data not shown) and showed a similar pattern of TRNOE effects: significant enhancements for the glycosylated residues, Thr3 and Ser4, and significant enhancements for residues Asp7, Thr8, Arg9, and Pro10 within the PDTRP epitope.

The pattern of TRNOE enhancements observed for the Tn3,Tn4-glycosylated 16mer in the presence of Fab closely mirrors the pattern of line broadening observed in the ^{1}H NMR-monitored titration of this glycopeptide (selective line broadening for the PDTRP peptide epitope and Tn carbohydrate resonances). This similarity in TRNOE and line broadening patterns suggests that both effects derive from increases in local correlation times (i.e., $\tau_B > \tau_F$; see eq 4) as the PDTRP peptide epitope and the Tn carbohydrates are preferentially bound and immobilized in the antibody combining site. Thus, the MUC1 B-cell epitope in the Tn3,Tn4-glycosylated 16mer appears to be comprised of two separate portions, a peptide epitope spanning the PDTRP sequence and a carbohydrate epitope consisting of Tn sugars attached at Thr3 and Ser4.

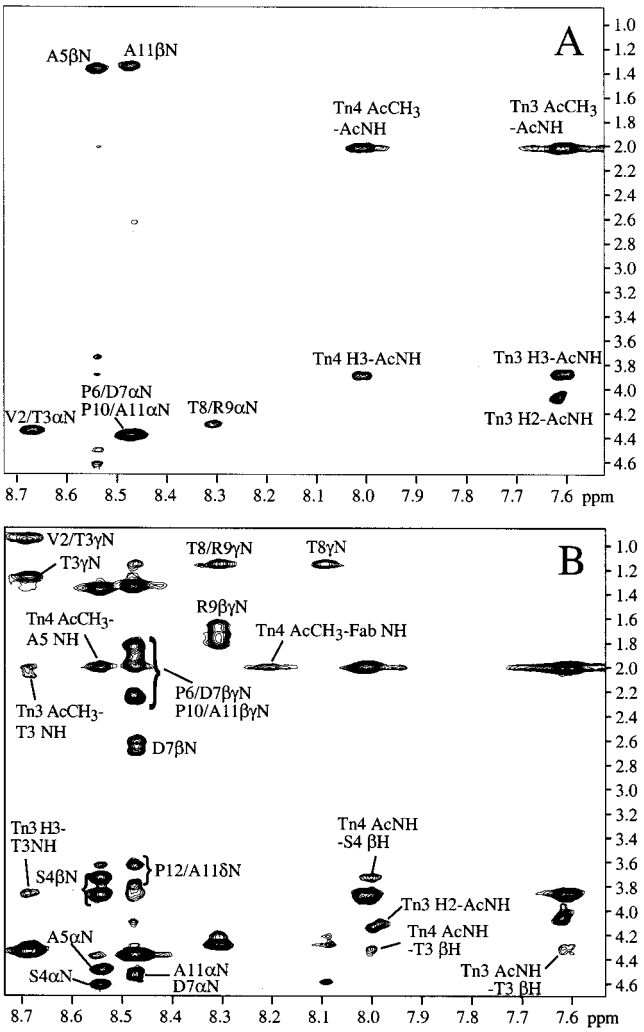

FIGURE 7: $d\alpha$N, $d\beta$N, $d\gamma$N, and $d\delta$N regions of NOESY spectra acquired at 25 °C from the reverse titration of the Tn3,Tn4-glycosylated MUC1 16mer with Fab B27.29. This figure illustrates the development of TRNOEs in the bound peptide, which are easier to identify at 25 °C due to the attenuation of the free peptide NOEs at this temperature. Panel A corresponds to 1.4 mM peptide (no Fab), whereas panel B corresponds to 200 μM Fab + 1.4 mM peptide (0.14 molar equiv of Fab/peptide). Experimental conditions were 90% H_2O/10% D_2O PBS buffer, pH 7.0, 25 °C.

TRNOESY experiments were also performed at 5 and 25 °C for the unglycosylated 16mer peptide in the presence of Fab B27.29 (data not shown). These experiments demonstrated TRNOE enhancements for residues within the PDTRP peptide epitope but no enhancements for residues at the C-terminus of the peptide, in agreement with the results obtained for the Tn3,Tn4-glycosylated 16mer. Significantly, no TRNOE enhancements were observed for either Thr3 or Ser4 in the unglycosylated peptide, presumably because these residues lack the attached carbohydrate that can bind directly to antibody.

Having mapped the B27.29 B-cell epitope in the glycosylated MUC1 antigen to separate peptide and carbohydrate epitopes, TRNOESY spectra were then carefully scrutinized for peptide−Fab and sugar−Fab NOEs. Figure 8 shows the dNN region of the NOESY/TRNOESY spectra acquired at

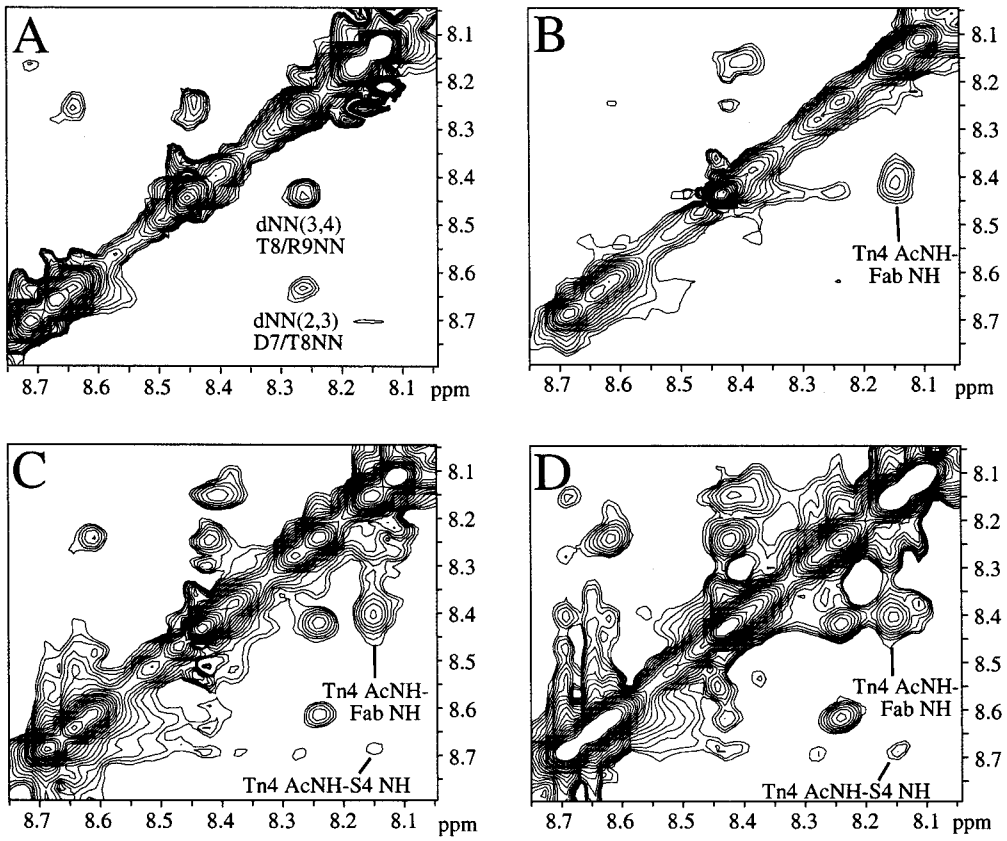

FIGURE 8: *d*NN regions of NOESY spectra acquired at 5 °C from the reverse titration of the Tn3,Tn4-glycosylated MUC1 16mer with Fab B27.29. Panel A corresponds to the 800 μM peptide (no Fab), panel B to 200 μM Fab + 400 μM peptide (0.5 molar equiv of Fab/peptide), panel C to 200 μM Fab + 800 μM peptide (0.25 molar equiv of Fab/peptide), and panel D to 200 μM Fab + 1.4 mM peptide (0.14 molar equiv of Fab/peptide). Experimental conditions were 90% H_2O/10% D_2O PBS buffer, pH 7.0, 5 °C.

5 °C from the reverse titration of the Tn3,Tn4-glycosylated 16mer and at four different molar equivalents of Fab. Panel A corresponds to no Fab (only peptide), panel B to 0.5 molar equiv of Fab/peptide, panel C to 0.25 molar equiv of Fab/peptide, and panel D to 0.14 molar equiv of Fab/peptide. These four ratios of Fab/peptide were explored so as to better discriminate peptide−peptide TRNOEs from intermolecular peptide−Fab and sugar−Fab NOEs. Examination of Figure 8 reveals an important sugar−Fab NOE, which is labeled Tn4 AcNH−Fab NH. This NOE is absent in both the free peptide (panel A) and the free Fab NOESY spectrum (not shown), confirming its source as sugar−Fab. The presence of such a strong and unequivocal sugar−Fab contact suggests a direct interaction of the Tn4 carbohydrate with Fab B27.29, supporting the line broadening and TRNOE results observed for this carbohydrate resonance.

Figure 9 shows the $d\beta$N and $d\gamma$N regions of the NOESY/TRNOESY spectra acquired at 5 °C from the same reverse titration of the Tn3,Tn4-glycosylated 16mer and using the same four molar equivalents of Fab described above. Another sugar−Fab NOE is observed in this figure, labeled Tn4 $AcCH_3$−Fab NH, which is absent in both the free peptide (panel A) and the free Fab NOESY spectrum. The Fab NH partner (at 8.41 ppm) in this Tn4 $AcCH_3$−Fab NH cross-peak is the same Fab NH in the Tn4 AcNH−Fab NH cross-peak shown in Figure 8, an assignment confirmed by temperature titrations. Panels C and D of Figure 9 also show a peptide−sugar TRNOE of special interest, Tn4 $AcCH_3$−T8 NH, which is absent in both the free peptide (panel A) and the free Fab NOESY spectrum (not shown). The existence of this medium-range peptide−sugar TRNOE implies that T8 and Tn4 are both bound at the antibody combining site and supports the notion that the MUC1 B-cell epitope is comprised of both a peptide portion and a carbohydrate portion. The simultaneous binding of T8 and Tn4 at the B27.29 combining site is supported by an analysis of all sugar−Fab and peptide−Fab NOEs observed in the reverse titration. These NOEs are listed in Table S6 and show Fab contacts to Tn3, Tn4, and T8 in the peptide. Of particular interest in Table S6 are the strong T8 $\gamma(CH_3)$−Fab NOEs linking the γ-methyl protons of Thr8 to an upfield Fab methyl group at −0.30 ppm (this peptide−Fab is observed at both 5 and 25 °C) and the strong T8 $\gamma(CH_3)$−Fab NOE linking the γ-methyl protons of Thr8 to aromatic Fab resonances at 6.91 ppm (observed at 25 °C). These NOEs identify Thr8 as a key Fab contact residue for the PDTRP peptide epitope.

Finally, turn-defining TRNOEs were carefully analyzed in the TRNOESY spectra of the Tn3,Tn4-glycosylated 16mer in order to determine if the type I β-turn found within the PDTRP core peptide epitope of the free peptide is conserved within the B27.29 combining site. Referring back to Figure 8, *d*NN(2,3) and *d*NN(3,4) connectivities diagnostic of turn conformation are observed both in the presence (panels C and D) and in the absence (panel A) of Fab. This implies that the β-turn conformation is conserved in the antibody-bound peptide. In addition, a careful examination of the two panels that represent the same concentration of peptide (panels A and C, respectively) shows modest 30% TRNOE enhancements for *d*NN(2,3) and *d*NN(3,4) in the presence of Fab, although the exact contributions of the free versus

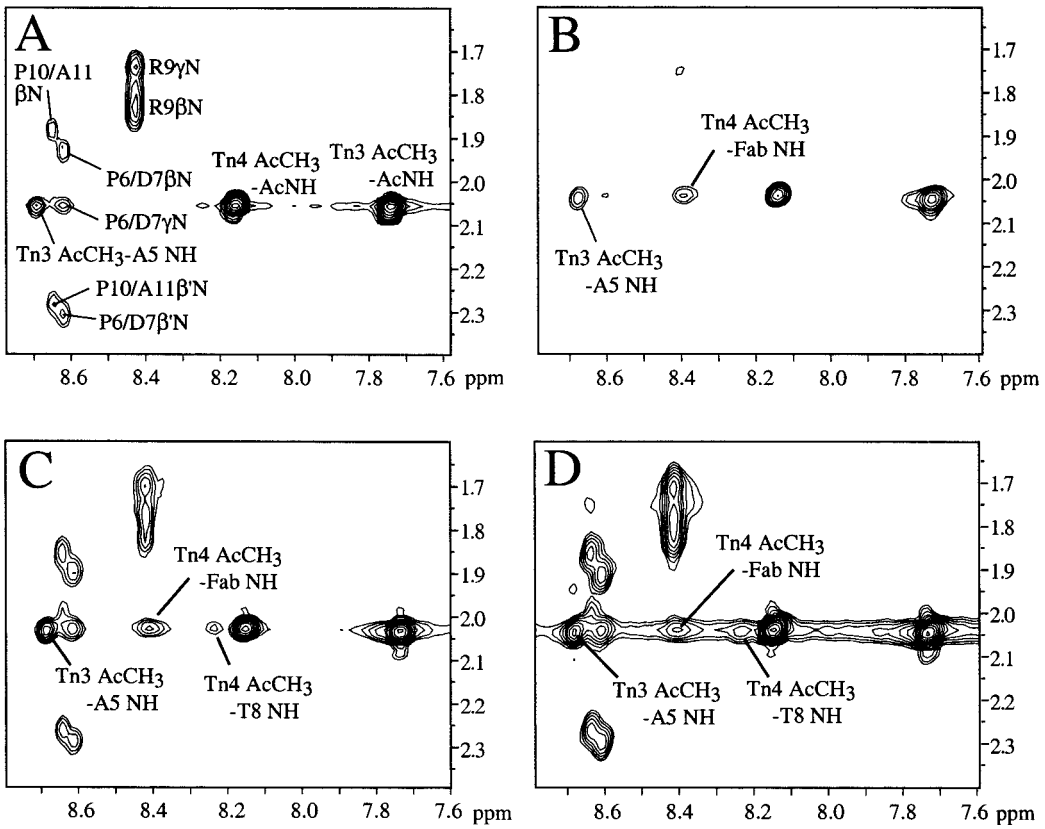

FIGURE 9: *dβ*N and *dγ*N regions of NOESY spectra acquired at 5 °C from the reverse titration of the Tn3,Tn4-glycosylated MUC1 16mer with Fab B27.29. Panel A corresponds to the 800 μM peptide (no Fab), panel B to 200 μM Fab + 400 μM peptide (0.5 molar equiv of Fab/peptide), panel C to 200 μM Fab + 800 μM peptide (0.25 molar equiv of Fab/peptide), and panel D to 200 μM Fab + 1.4 mM peptide (0.14 molar equiv of Fab/peptide). Experimental conditions were 90% H_2O/10% D_2O PBS buffer, pH 7.0, 5 °C.

the bound state to these observed TRNOEs are difficult to quantitate. However, coupling constant and temperature coefficient measurements made for the Tn3,Tn4-glycosylated 16mer in the presence of 0.4 molar equiv of Fab B27.29 (see Table S7B) do support a small increase in turn population in the bound state: Fab binding leads to a decrease in the $^3J_{N\alpha}$ coupling constant of Asp7 (5.9 to 5.4 Hz) and a decrease in the $-\Delta\delta/\Delta T$ of Arg9 (6.0 to 5.2 ppb/K). Future studies by the group will involve isotope-edited and isotope-filtered experiments of labeled MUC1 peptides binding to Fab, so as to better define the involvement of the PDTR β-turn in MUC1 humoral immune recognition and to better map the antibody binding interface on the MUC1 antigen.

Modeling of a Proposed Antibody Binding Interface on the MUC1 Glycopeptide. A model of a proposed binding interface on the Tn3,Tn4-glycosylated 16mer has been generated on the basis of the peptide−Fab and sugar−Fab NOEs observed for the peptide in the presence of Fab B27.29 (see Table S6). The model assumes a type I β-turn spanning residues Pro6-Asp7-Thr8-Arg9 and a polyproline type II helix for the C-terminal half of the peptide (Pro10−Ala16) (see Experimental Procedures). Two CPK space-filled views of the model are shown in Figure 10, related by a 40° rotation around a horizontal axis. The Tn carbohydrates (Tn3 and Tn4) and the Thr8 side chain are arranged on the same face of the glycopeptide so as to allow a contiguous surface for binding to B27.29. White atoms correspond to hydrogens and their directly attached heteroatoms for which peptide−Fab [T8 αH−Fab, T8 $\gamma(CH_3)$−Fab] and sugar−Fab NOEs (Tn3 AcNH−Fab, Tn4 AcNH−Fab, Tn4 $AcCH_3$−Fab) were observed. While the model is not intended to substitute for a rigorous structure calculation of the Fab-bound glycopeptide, it does serve to illustrate that peptide and carbohydrate portions of the MUC1 glycopeptide can contribute to a structurally contiguous B27.29 B-cell epitope.

CONCLUSIONS

The cryptic core carbohydrates that remain on the underglycosylated MUC1-expressing tumor are believed to contribute significantly to humoral immune recognition of the tumor (*50*, *73*−*76*). However, the mechanism through which this occurs is not yet well understood, especially as an exact glycosylation state (if there is only one) of the MUC1-expressing tumor remains to be determined. In the absence of a clear picture of the tumor-associated glycosylation state, we advance two plausible mechanisms to explain how MUC1 carbohydrate might contribute to humoral immune recognition of the intact tumor. In the first of these mechanisms, the cryptic carbohydrates are proposed to affect MUC1 humoral immune recognition by altering the conformation of the PDTRP peptide epitope portion of the MUC1 antigen. In the second of these mechanisms, the cryptic carbohydrates are proposed to affect MUC1 humoral immune recognition by directly interacting with the B-cell receptor.

To explore the first of these mechanisms, that carbohydrates alter the conformation of the PDTRP core peptide epitope, NMR studies were performed, probing the structural and dynamical effects of glycosylation in a series of synthetic MUC1 glycopeptides of the form (Gly1-Val2-Thr3-Ser4-

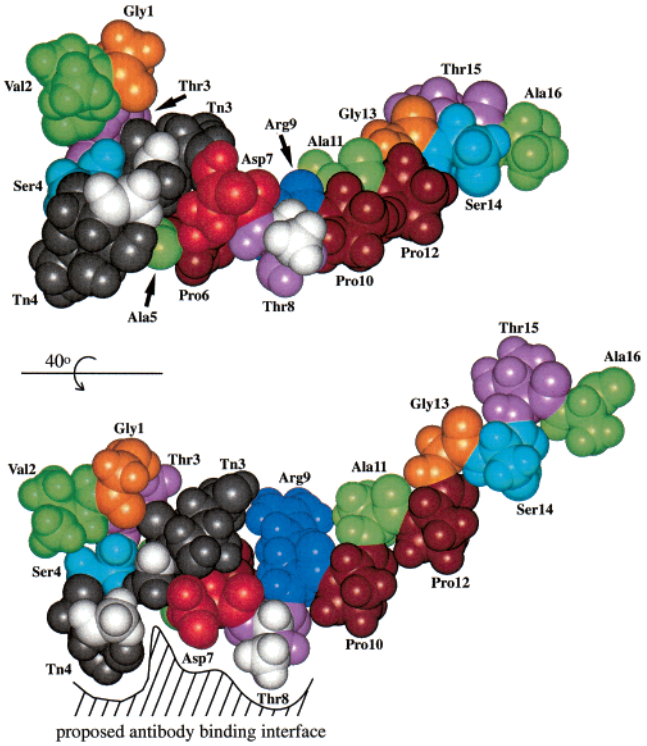

FIGURE 10: CPK space-filled model of the Tn3,Tn4-glycosylated MUC1 16mer peptide showing a proposed antibody binding interface, based on the peptide−Fab and sugar−Fab NOEs observed for the peptide in the presence of Fab B27.29 (see Table S6). Two views of the model are shown, related by a 40° rotation around a horizontal axis. The amino acid backbones and side chains are color coded (Gly = orange; Val and Ala = green; Pro = brown; Asp = red; Arg = blue; Thr = violet; Ser = cyan). The Tn3 and Tn4 carbohydrates are colored gray. White atoms correspond to hydrogens and their directly attached heteroatoms for which peptide−Fab [T8 αH−Fab, T8 $\gamma(CH_3)$−Fab] and sugar−Fab NOEs (Tn3 AcNH−Fab, Tn4 AcNH−Fab, Tn4 $AcCH_3$−Fab) were observed (see Table S6). Asp7, situated in the middle of the binding pocket in the model, is significantly line broadened in the presence of Fab, which may account for the lack of observable peptide−Fab NOEs to this residue.

Ala5-Pro6-Asp7-Thr8-Arg9-Pro10-Ala11-Pro12-Gly13-Ser14-Thr15-Ala16). The results of these studies showed that Tn3,Tn4 glycosylation at Thr3 and Ser4 produced only localized effects on the conformation and backbone dynamics of residues at or immediately adjacent to the site(s) of carbohydrate attachment. No longer range effects on the conformation and dynamics of the downstream type I β-turn that spans residues Pro6-Asp7-Thr8-Arg9 within the core peptide epitope were observed. These results suggest that the increased affinity displayed by the Tn3,Tn4-glycosylated MUC1 peptide for the anti-MUC1 antibody B27.29 (*50*) is not caused by the carbohydrate stabilizing a peptide epitope conformation most favored for binding (presumably the type I β-turn).

To explore the second mechanism, that the MUC1 carbohydrates contribute to MUC1 humoral immunogenicity by directly binding to the B-cell receptor, two-dimensional ^{1}H TRNOESY experiments of the binding of the Tn3,Tn4-glycosylated MUC1 16mer to the Fab fragment of B27.29 were performed. The results of these studies showed that the B27.29 MUC1 B-cell epitope maps to two separate parts of the glycopeptide, the core peptide epitope spanning the PDTRP sequence and a second carbohydrate epitope comprised of the Tn moieties attached at Thr3 and Ser4. Careful analysis of intermolecular sugar−Fab and peptide−Fab NOEs observed in the TRNOESY also showed that the Tn4 carbohydrate and the Thr8 side chain directly contact the Fab across the combining site interface, defining separate carbohydrate and peptide "contact points". Finally, turn-defining peptide−peptide TRNOEs observed in the TRNOESY spectra are consistent with the PDTRP peptide epitope maintaining its free solution state β-turn conformation in the B27.29 combining site. Taken together, these results point to the involvement of the PDTR β-turn and the upstream cryptic Tn carbohydrates in the humoral immune recognition of the underglycosylated MUC1 tumor in vivo.

Significance of Results to MUC1 Glycopeptide Vaccine Design. Several lines of evidence suggest that the key to boosting MUC1 specific immunity in adenocarcinoma patients may be the inclusion of the MUC1 tumor-associated carbohydrates at select sites in the MUC1 peptide vaccine. Exposure of these tumor-associated core carbohydrate epitopes through the use of O-glycosylation inhibitors has been shown to lead to lysis of MUC1 transfected targets in a Class I MHC-restricted manner (*77*). In addition, immunization trials using MUC1 carbohydrate epitopes alone (no peptide) can elicit both a cytotoxic response against the MUC1-expressing tumor and a protective effect against further tumor challenge in mice (*78*, *79*). These results suggest that preferential killing of MUC1-expressing tumors may be due to the T-cell recognition of an internal carbohydrate epitope accessible only on the underglycosylated MUC1. Furthermore, natural MUC1 antibodies from breast cancer patients have been shown to react more strongly with Tn-glycosylated peptides than with the naked peptide sequence (*76*), implying that a Tn-glycosylated MUC1 peptide more closely approximates the mucin epitope as it exists on the partially glycosylated tumor cell surface. All of these results indicate that a MUC1 glycopeptide might make a better vaccine candidate than its unglycosylated counterpart.

In the present study, we have shown that the inclusion of the tumor-associated Tn carbohydrates at Thr3 and Ser4 upstream from the PDTRP core peptide epitope (GVTSAP-DTRPAPGSTA) increases B27.29 binding affinity through direct carbohydrate−antibody interactions. These results demonstrate that proximal carbohydrate and peptide structural epitopes are part of the recognition domain for B27.29, whose natural tumor-associated antigen is extensively glycosylated with "cryptic" carbohydrate structures but also underglycosylated in the region of the PDTRP core peptide epitope. Future studies by this group will involve other MUC1 glycoforms, so as to arrive at a more detailed understanding of the conformation and glycosylation state of the MUC1 antigen as it exists on the tumor cell surface. This work should ultimately provide information relevant to the design of a more potent and immunospecific MUC1 glycopeptide vaccine.

ACKNOWLEDGMENT

The authors thank Dr. Brian D. Sykes for the use of NMR, computer, and wet laboratory facilities and Dr. William M. Atkins for the use of spectrofluorometers and wet laboratory facilities for performing the fluorescence measurements of the MUC1 16mer peptides and glycopeptides binding to Fab B27.29.

SUPPORTING INFORMATION AVAILABLE

Eight tables of NMR data measured for the unglycosylated and Tn-glycosylated MUC1 16mer peptides: ^{1}H and ^{13}C NMR resonance assignments (Tables S1 and S2); coupling constants, temperature coefficients, and $^{1}H\alpha$ and $^{13}C\alpha$ chemical shift indexes (Table S3); ^{13}C NMR relaxation data (Table S4); peptide−sugar NOEs (Table S5); peptide−Fab and sugar−Fab NOEs (Table S6); temperature coefficients and coupling constants measured in the presence of Fab (Table S7); and peptide−sugar NOEs measured in the presence of Fab (Table S8). This material is available free of charge via the Internet at http://pubs.acs.org.

REFERENCES

1. Taylor-Papadimitriou, J., Burchell, J., Miles, D. W., and Dalziel, M. (1999) *Biochim. Biophys. Acta 1455*, 301−313.
2. Miles, D. W., and Taylor-Papadimitriou, J. (1999) *Pharmacol. Ther. 82*, 97−106.
3. Apostolopoulos, V., Sandrin, M. S., and McKenzie, I. F. (1999) *J. Mol. Med. 77*, 427−436.
4. Apostolopoulos, V., Pietersz, G. A., and McKenzie, I. F. (1999) *Curr. Opin. Mol. Ther. 1*, 98−103.
5. Van den Steen, P., Rudd, P. M., Dwek, R. A., and Podenakker, G. (1998) *Crit. Rev. Biochem. Mol. Biol. 33*, 151−208.
6. Rudd, P. M., and Dwek, R. A. (1997) *Crit. Rev. Biochem. Mol. Biol. 32*, 1−100.
7. Carlstedt, I., and Davies, J. R. (1997) *Biochem. Soc. Trans. 25*, 214−219.
8. Koganty R. R., Reddish M. A., and Longenecker, B. M. (1997) in *Glycopeptides and Related Compounds: Synthesis, Analysis and Application* (Large, D. G., and Warren, C. D., Eds.) pp 707−743, Dekker, New York.
9. Hanisch, F. G. (2001) *Biol. Chem. 382*, 143−149.
10. Girling, A., Bartkova, J., Burchell, J., Gendler, S., Gillett, C., and Taylor-Papadimitriou, J. (1989) *Int. J. Cancer 43*, 1072−1076.
11. Burchell, J., Taylor-Papadimitriou, J., Boshell, M., Gendler, S., and Duhig, T. (1989) *Int. J. Cancer 44*, 691−696.
12. Xing, P. X., Prenzoska, J., and McKenzie, I. F. (1992) *Mol. Immunol. 29*, 641−650.
13. Xing, P. X., Prenzoska, J., Quelch, K., and McKenzie, I. F. (1992) *Cancer Res. 52*, 2310−2317.
14. Denton, G., Sekowski, M., and Price, M. R. (1993) *Cancer Lett. 70*, 143−150.
15. Kotera, Y., Fontenot, J. D., Pecher, G., Metzgar, R. S., and Finn, O. J. (1994) *Cancer Res. 54*, 2856−2860.
16. Bashford, J. L., Robins, R. A., and Price, M. R. (1993) *Int. J. Cancer 54*, 778−783.
17. Itzkowitz, S. H., Yuan, M., Montgomery, C. K., Kjeldsen, T., Takahashi, H. K., Bigbee, W. L., and Kim, Y. S. (1989) *Cancer Res. 49*, 197−204.
18. Brockhausen, I., Yang, J., Dickinson, N., Ogata, S., and Itzkowitz, S. H. (1998) *Glycoconjugate J. 15*, 595−603.
19. Cao, Y., Karsten, U., Otto, G., and Bannasch, P. (1999) *Virchows. Arch. 434*, 503−509.
20. Cao, Y., Schlag, P. M., and Karsten, U. (1997) *Virchows. Arch. 431*, 159−166.
21. Springer, G. F. (1997) *J. Mol. Med. 75*, 594−602.
22. Springer, G. F. (1995) *Crit. Rev. Oncog. 6*, 57−85.
23. Kishikawa, T., Ghazizadeh, M., Sasaki, Y., and Springer, G. F. (1999) *Jpn. J. Cancer Res. 90*, 326−232.
24. Terasawa, K., Furumoto, H., Kamada, M., and Aono, T. (1996) *Cancer Res. 56*, 2229−2232.
25. David, L., Nesland, J. M., Clausen, H., Carneiro, F., and Sobrinho-Simoes, M. (1992) *APMIS, Suppl. 27*, 162−172.
26. Nishimori, I., Perini, F., Mountjoy, K. P., Sanderson, S. D., Johnson, N., Cerny, R. L., Gross, M. L., Fontenot, J. D., and Hollingsworth, M. A. (1994) *Cancer Res. 54*, 3738−3744.
27. Nishimori, I., Johnson, N. R., Sanderson, S. D., Perini, F., Mountjoy, K. P., Cerny, R. L., Gross, M. L., and Hollingsworth, M. A. (1994) *J. Biol. Chem. 269*, 16123−16130.
28. Wandall, H. H., Hassan, H., Mirgorodskaya, E., Kristensen, A. K., Roepstorff, P., Bennett, E. P., Nielsen, P. A., Hollingsworth, M. A., Burchell, J., Taylor-Papadimitriou, J., and Clausen, H. (1997) *J. Biol. Chem. 272*, 23503−23514.
29. Müller, S., Goletz, S., Packer, N., Gooley, A., Lawson, A. M., and Hanisch, F.-G. (1997) *J. Biol. Chem. 272*, 24780−24798.
30. Müller, S., Alving, K., Peter-Katalinic, J., Zacharas, N., Gooley, A., and Hanisch, F.-G. (1999) *J. Biol. Chem. 274*, 18165−18172.
31. Schuman, J., Koganty, R. R., Longenecker, B. M., and Campbell, A. P. (2002) *J. Pept. Res.* (submitted for publication).
32. Reddish, M. D., Helbrecht, N., Almeida, A. F., Madiyalakan, R., Suresh, M. R., and Longenecker, B. M. (1992) *J. Tumor Maker Oncol. 7*, 19−27.
33. Schol, D. J., Meulenbroek, M. F. A., Snijdewint, F. G. M., von Mansdorff-Pouilly, S., Verstraeten, R. A., Murakami, F., Kenemans, P., and Hilgers J. (1998) *Tumor Biol. 19*, 35−45.
34. MacLean, G. D., Reddish, M A., and Longenecker, B. M. (1997) *J. Immunother. 20*, 70−78.
35. States, D. J., Haberkorn, R. A., and Ruben, D. J. (1982) *J. Magn. Reson. 48*, 286−292.
36. Piatini, U., Sorenson, O. W., and Ernst, R. R. (1982) *J. Am. Chem. Soc. 104*, 6800−6801.
37. Rance, M., Sorenson, O. W., Bodenhausen, G., Wagner, G., Ernst, R. R., and Wüthrich, K. (1983) *Biochem. Biophys. Res. Commun. 117*, 479−485.
38. Bax, A., and Davis, D. G. (1985) *J. Magn. Reson. 65*, 355−360.
39. Jeener, J., Meier, B. H., Bachmann, P., and Ernst, R. R. (1979) *J. Chem. Phys. 71*, 4546−4553.
40. Macura, S., and Ernst, R. R. (1980) *Mol. Phys. 41*, 95−117.
41. Delaglio, F., Grzesiek, S., Vuister, G. W., Zhu, G., Pfeifer, J., and Bax, A. (1995) *J. Biomol. NMR 6*, 277−293.
42. Yamakazi, T., Muhandiram, R., and Kay, L. E. (1994) *J. Am. Chem. Soc. 116*, 8266−8278.
43. Karanikas, V., Patton, K., Jamieson, G., Pietersz, G., and McKenzie, I. (1997) *Tumor Biol. 19*, 71−78.
44. Nice, E. C., McInerney, T. L., and Jackson, D. C. (1996) *Mol. Immunol. 33*, 659−670.
45. Gemmecker, G. (1999) NMR Spectroscopy in Drug Development and Analysis in *NMR as a Tool in Drug Research* (Holzgrabe, U., Wawer, I., and Diehl, B., Eds.) Chapter 9, pp 140−141, John Wiley and Sons, New York.
46. Campbell, A. P., and Sykes, B. D. (1993) *Annu. Rev. Biophys. Biomol. Struct. 22*, 99−122.
47. Fontenot, J. D., Finn, O. J., Dales, N., Andrews, P. C., and Montelaro, R. C. (1993) *Pept. Res. 6*, 330−336.
48. Fontenot, J. D., Tjandra, N., Bu, D., Ho, C., Montenaro, R. C., and Finn, O. J. (1993) *Cancer Res. 53*, 5386−5394.
49. Fontenot, J. D., Mariappan, S. V., Catasti, P., Domenech, N., Finn, O. J., and Gupta, G. (1995) *J. Biomol. Struct. Dyn. 13*, 245−260.
50. Liu, X., Sejbal, J., Kotovych, G., Koganty, R., Reddish, M. A., Jackson, L., Gandhi, S. S., Mendoca, A. J., and Longenecker, B. M. (1995) *Glycoconjugate J. 12*, 607−617.
51. Wishart, D. S., Sykes, B. D., and Richards, F. M. (1991) *J. Mol. Biol. 222*, 311−333.
52. Wishart, D. S., Bigam, C. G., Holm, A., Hodges, R. S., and Sykes, B. D. (1995) *J. Biomol. NMR 5*, 67−81.
53. Wüthrich, K. (1986) in *NMR of Proteins and Nucleic Acids*, John Wiley and Sons, New York.
54. Chandrasekhar, K., Profy, A. T., and Dyson, H. J. (1991) *Biochemistry 30*, 9187−9194.
55. Scanlon, M. J., Morley, S. D., Jackson, D. E., Price, M. R., and Tendler, S. J. B. (1992) *Biochem. J. 283*, 137−144.
56. Kirnarsky, L., Prakash, O., Vogen, S. M., Nomoto, M., Hollingsworth, M. A., and Sherman, S. (2000) *Biochemistry 39*, 12076−12082.
57. Richardson, J. S. (1981) *Adv. Protein Chem. 34*, 167−339.
58. Wilmot, C. M., and Thornton, J. M. (1988) *J. Mol. Biol. 203*, 221−232.
59. Gupta, A., and Chauhan, V. S. (1990) *Biopolymers 30*, 395−403.
60. Inai, Y., Kurashima, S., Hirabayashi, T., and Yokota, K. (2000) *Biopolymers 53*, 484−496.
61. MacArthur, M. W., and Thornton, J. M. (1991) *J. Mol. Biol. 218*, 397−412.
62. Yao, J., Feher, V. A., Espejo, B. F., Reymond, M. T., Wright, P. E., and Dyson, H. J. (1994) *J. Mol. Biol. 243*, 736−753.
63. Campbell, A. P., McInnes, C., Hodges, R. S., and Sykes, B. D. (1995) *Biochemistry 34*, 16255−16268.
64. Rose, G. D., Gierasch, L. M., and Smith, J. A. (1985) *Adv. Protein Chem. 37*, 1−109.
65. Andersen, N. H., Neidigh, J. W., Harris, S. M., Lee, G. M., Liu, Z., and Tong, H. (1997) *J. Am. Chem. Soc. 119*, 8547−8561.

66. Mimura, Y., Inoue, Y., Maeji, N. J., and Chujo, R. (1989) *Int. J. Pept. Protein Res. 34*, 363−368.
67. Gerken, T. A., Butenhof, K. J., and Shogren, R. (1989) *Biochemistry 28*, 5536−5543.
68. Live, D. H., Williams, L. J., Kuduk, S. D., Schwarz, J. B., Glunz, P. W., Chen, X. T., Sames, D., Kumar, R. A., and Danishefsky, S. J. (1999) *Proc. Natl. Acad. Sci. U.S.A. 96*, 3489−3493.
69. Liang, R., Adreotti, A. H., and Kahne, D. (1995) *J. Am. Chem. Soc. 117*, 10395−10396.
70. Cheetham, J. C., Raleigh, D. P., Griest, R. E., Redfield, C., Dobson, C. M., and Rees, A. R. (1991) *Proc. Natl. Acad. Sci. U.S.A. 88*, 7968−7972.
71. Zvi, A., Kustanovich, I., Feigelson, D., Levy, R., Eisenstein, M., Matsushita, S., Richalet-Sécordel, P., Regenmortel, M. H. V., and Anglister, J. (1995) *Eur. J. Biochem. 229*, 178−187.
72. Campbell, A. P., Wong, W. Y., Houston, M. E. Jr., Schweizer, F., Cachia, P. J., Irvin, R. T., Hindsgaul O., Hodges, R. S., and Sykes, B. D. (1997) *J. Mol. Biol. 267*, 382−402.
73. Spencer, D. I., Missailidis, S., Denton, G., Murray, A., Brady, K., Matteis, C. I., Searle, M. S., Tendler, S. J., and Price M. R. (1999) *Biospectroscopy 5*, 79−91.
74. Spencer, D. I. R., Price, M. R., Tendler, S. J. B., De Matteis, C. I., Standie, T., and Hanisch, F.-G. (1996) *Cancer Lett. 100*, 11−15.
75. Karsten, U., Diotel, C., Klich, G., Paulsen, H., Goletz, S. Müller, S., and Hanisch, F.-G. (1998) *Cancer Res. 58*, 2541−2549.
76. von Mensdorff-Pouilly, S., Petrakou, E., Kenemans, P., van Uffelen, K., Verstraeten, A. A., Snijdewint, F. G., van Kamp, G. J., Schol, D. J., Reis, C. A., Price, M. R., Livingston, P. O., and Hilgers, J. (2000) *Int. J. Cancer 86*, 702−712.
77. Böhm, C. M., Mulder, M. C., Zennadi, R., Notter, M., Schmitt-Graff, A., Finn, O. J., Taylor-Papadimitriou, J., Stein, H., Clausen, H., Riecken, E. O., and Hanski, O. (1997) *Scand. J. Immunol. 46*, 27−34.
78. Henningsson, C. M., Selvaraj, S., MacLean, G. D., Suresh, M. R., Noujaim, A. A., and Longenecker, B. M. (1987) *Cancer Immunol. Immunother. 25*, 231−241.
79. Fung, P. Y. S., Madej, M., Koganty, R. R., and Longenecker, B. M. (1990) *Cancer Res. 50*, 4308−4314.

BI012176Z